THE GEOLOGICAL SOCIETY OF AMERICA®

Isotopic constraints on the peak of the Early Paleozoic Icehouse

Joshua B. Zimmt[1,2,†,*], Kristin D. Bergmann[3,*], Seth Finnegan[1,4], Theodore M. Present[5], Adam B. Jost[3], and André Desrochers[6]

[1]*University of California Museum of Paleontology and Department of Integrative Biology, University of California, Berkeley, California 94720, USA*

[2]*Department of Earth and Planetary Sciences, McGill University, Montreal, Quebec H3A 0E8, Canada*

[3]*Department of Earth, Atmospheric and Planetary Sciences, Massachusetts Institute of Technology, Cambridge, Massachusetts 02139, USA*

[4]*Smithsonian Tropical Research Institute, Panama City, Panamá Province 0843-03092, Panama*

[5]*Division of Geological and Planetary Sciences, California Institute of Technology, Pasadena, California 91125, USA*

[6]*Department of Earth and Environmental Sciences, University of Ottawa, Ottawa, Ontario K1N 6N5, Canada*

ABSTRACT

While the intensification of the Early Paleozoic Icehouse is commonly cited as the main driver of the Late Ordovician mass extinction, we lack high-resolution, stratigraphically constrained climate records to test this hypothesis. Here, we develop a high-resolution climate record for the Late Ordovician by applying stable isotope geochemistry ($\delta^{18}O$, $\delta^{13}C$; n = 81) and carbonate clumped isotope paleothermometry (Δ_{47}; n = 45) to fossils from the stratigraphically expanded Ellis Bay Formation on Anticosti Island (Canada). Focusing our analysis on fossils that primarily experienced closed-system alteration, we identify two distinct phases of increasing fossil $\delta^{18}O_{VPDB}$ values: a moderate increase of 1.0‰–1.5‰ across the Katian/Hirnantian boundary and a larger increase of 2.5‰–4.5‰ in the middle to late Hirnantian. Only the latter is associated with Δ_{47} evidence for cool tropical sea surface temperatures, and based on its sequence stratigraphic context immediately overlying a regional subaerial unconformity, we interpret this excursion as reflecting the earliest stages of transgression during the waning of the Hirnantian Glacial Maximum. This revises the conclusions of previous paired stable and clumped isotope studies, which argued that the major drop in sea surface temperatures occurred at the Katian/Hirnantian boundary. When integrated with patterns of faunal turnover from Anticosti Island, our conclusion that major tropical cooling and maximum ice volumes did not occur until the middle to late Hirnantian suggests that an apparent pulse of extinction near the Katian/Hirnantian boundary may be in part a stratigraphic artifact generated by widespread glacio-eustically forced unconformities and facies shifts.

INTRODUCTION

Icehouse climates are infrequent events throughout Earth history and are often associated with major transitions in the history of life (Trotter et al., 2008; Montañez and Poulsen, 2013; Judd et al., 2024). While the dynamics of the most recent, late Cenozoic icehouse are relatively well understood (Zachos et al., 2001; Westerhold et al., 2020), an understanding of pre-Cenozoic icehouses is hampered by a paucity of deep-sea records, biased representation of shelf environments, and diagenetic alteration of proxy records (Pope and Read, 1998; Swart, 2008; Higgins et al., 2018; Peters et al., 2018; Jones et al., 2020; Goldberg et al., 2021). More specifically, our understanding of the first Phanerozoic icehouse, the Early Paleozoic Icehouse (Page et al., 2007), remains incomplete due to all of these factors. Early studies proposed that the icehouse was a brief but intense episode confined to the Hirnantian Stage, consisting of a single episode of icesheet growth and glacio-eustatic drawdown (Brenchley and Štorch, 1989; Brenchley et al., 1994; Armstrong and Coe, 1997; Ghienne, 2003). Subsequent sequence stratigraphic, cyclo-stratigraphic, and geochemical analyses, as well as computational modeling, have revealed that the dynamics of the Early Paleozoic Icehouse were far more complex (Elrick et al., 2013; Ghienne et al., 2014; Pohl et al., 2016; Sinnesael et al., 2021; Zimmt et al., 2024; Bergmann et al., 2025), and there is a growing body of literature suggesting that the Early Paleozoic Icehouse may have begun earlier, largely based on physical stratigraphic evidence (Calner et al., 2010; Turner et al., 2012; Ghienne et al., 2023). While uncertainty remains about the timing of the Ordovician greenhouse–icehouse transition, studies of Ordovician/Silurian boundary intervals worldwide identify a clear glacial maximum in the Hirnantian Stage, characterized by rapid and substantial cooling of tropical seas and the growth of Gondwanan ice sheets (Vandenbroucke et al., 2010; Finnegan et al., 2011; Pohl et al., 2016), and a major (>100 m) drop in eustatic sea level (Harris et al., 2004; Kaljo et al., 2008; Finnegan et al., 2011; Porębski et al., 2019; Goldberg et al., 2021; Ghienne et al., 2023).

The Hirnantian Glacial Maximum (peak of the Early Paleozoic Icehouse) is often cited as the cause of a number of disruptions to the Earth system, including a large positive excursion in both carbonate and organic $\delta^{13}C$ (the Hirnantian Isotopic Carbon Excursion or HICE; Brenchley et al., 1994; Kump et al., 1999; Chen et al., 2006; Melchin and Holmden, 2006; Jones et al., 2011), the reorganization of ocean circulation and redox conditions (Hammarlund et al., 2012; Melchin et al., 2013; Bartlett et al., 2018; Zou et al., 2018; Young et al., 2020; Li et al., 2021a; Pohl et al., 2021; Kozik et al., 2022), and the Late Ordovician mass extinction (LOME), which eliminated an estimated ~85% of marine species diversity globally (Jablonski, 1991; Sheehan, 2001; Harper et al., 2014; Rong et al., 2020; Saupe et el., 2020; Rasmussen et al., 2019, 2023). However, a well-

Joshua B. Zimmt https://orcid.org/0000-0002-3960-283X
[†]josh_zimmt@berkeley.edu
[*]Co-first authors

GSA Bulletin;
Published online 23 June 2025

https://doi.org/10.1130/B37897.1.

resolved causal relationship between the Early Paleozoic Icehouse, oceanographic change, carbon cycling, and the LOME remains elusive.

Classically, the LOME has been interpreted as two distinct pulses of extinction—the first, and main, pulse associated with cooling and glacio-eustatic fall at the Katian/Hirnantian boundary, and the second, smaller pulse associated with warming and glacio-eustatic rise in the middle to late Hirnantian (Sheehan., 2001; Finnegan et al., 2012; Saupe et al., 2020)—but it is now better recognized that the overarching control of relative sea level changes on stratigraphic architecture strongly influences both the preservation and expression of the history of life in the fossil record (Holland, 1995; Peters, 2005; Nawrot et al., 2018; Zimmt et al., 2021). Stratigraphic architecture can also hamper an interpretation of the sequence of environmental changes from geochemical proxy records (Swart, 2008; Jones et al., 2020; Geyman and Maloof, 2021), particularly in icehouse records like the Hirnantian that are characterized by complex shingling of stratigraphic sequences, unconformities, and large offsets in facies (Kidwell, 1997; Read, 1998; Pope and Read, 1998; Brenchley et al., 2003; Fielding et al., 2006; Di Celma and Cantalamessa, 2007). Interpretation of the oxygen isotope record, which is particularly critical for constraining the timing and magnitude of climate change, is additionally complicated by its susceptibility to diagenetic alteration through interaction with meteoric and basinal fluids, particularly under icehouse conditions, as fluid-buffered alteration mechanisms become more dominant due to frequent, large amplitude sea level changes (Ahm et al., 2017, 2018; Higgins et al., 2018; Jones et al., 2020).

Here we assess the timing and magnitude of the Hirnantian Glacial Maximum and its compatibility with the traditional model of the Late Ordovician mass extinction by applying stable isotope geochemistry ($\delta^{18}O$, $\delta^{13}C$) and carbonate clumped isotope paleothermometry (Δ_{47}) to fossils from the Ellis Bay Formation (Anticosti Island, Québec, Canada). After screening for diagenetic alteration, the population of Δ_{47} temperatures from fossils suggests variable closed-system alteration processes (viz., sediment-buffered diagenesis and solid-state reordering), which re-equilibrated ^{13}C–^{18}O bonding while largely preserving the original fossil $\delta^{18}O$ signatures, alongside less extensive open-system alteration under fully marine conditions. Using isotopic and trace element data to restrict our analysis to fossils with the best preserved $\delta^{18}O$ signatures, we find evidence of two phases of increasing $\delta^{18}O$ values within the Upper Ordovician strata on Anticosti Island, the younger of which represents the Hirnantian Glacial Maximum. Compared to data compiled from late Katian fossils from the underlying Vaureal Formation, the total excursion reflects an ~3.5‰–5.5‰ increase in fossil $\delta^{18}O_{VPDB}$ values, concurrent with a drop in Δ_{47} temperatures. These, however, represent a lower limit on the effects of both tropical sea surface cooling and ice sheet growth associated with the Early Paleozoic Icehouse. Given these new data, if the first "pulse" of the LOME was indeed driven by an abrupt cooling of tropical sea surface temperatures and glacio-eustatic fall, as the current understanding of the extinction event suggests, it would have occurred well after the Katian/Hirnantian boundary in the Anticosti Basin, calling into question the traditional two-pulse model of the mass extinction.

GEOLOGIC BACKGROUND

Ordovician/Silurian strata exposed along the northwest-southeast–trending outcrop belt of Anticosti Island (Québec, Canada; Figs. 1A and 1B) record deposition in proximal ramp settings on the landward side of the Anticosti Basin, a foreland basin along the margin of the St. Lawrence Platform (Sanford, 1993). During the Late Ordovician, the Anticosti Basin was located along the southeastern margin of Laurentia, between 20°S and 30°S paleolatitude (McLaughlin and Brett, 2007; Torsvik and Cocks, 2016; Swanson-Hysell and Macdonald, 2017). Throughout the Ordovician, elevated subsidence rates associated with the initial emplacement of the Taconic thrust sheet led to the accumulation of an ~2000-m-thick (~900 m exposed) stratigraphic succession (Long, 2007; McLaughlin et al., 2016), comprising one of the thickest Ordovician/Silurian boundary sections in the world. Despite long-lived tectonic activity along the eastern margin of North America, the exposed succession on Anticosti Island is relatively undeformed compared to the rest of the continental margin, with only minor faults and folds associated with later tectonic activity (Bordet et al., 2010; Pinet et al., 2012). The Upper Ordovician and Lower Silurian parts of the succession are particularly well preserved along the western half of the island, with peak burial temperatures likely less than 80 °C as constrained by (U-Th)/He thermochronology (Powell et al., 2018) and conodont alteration index (CAI <1; Nowlan and Barnes, 1987), making the succession a valuable climatic and environmental archive.

Facies throughout the succession reflect storm-controlled deposition in shallow marine settings, reflecting the position of the basin within the tropical storm belt (Sami and Desrochers, 1992; Long, 2007; Desrochers et al., 2010; Copper et al., 2013; Copper and Jin, 2014; Zimmt et al., 2024). Both the Upper Ordovician Vaureal and Ellis Bay formations (Schuchert and Twenhofel, 1910) preserve a series of mixed carbonate–siliciclastic facies, which in the present-day western part of the island consists of an association of deeper-water facies comprising lime mudstones and shales that is capped by a shallow-water facies association within the uppermost Lousy Cove and Laframboise members (Petryk, 1981; Long and Copper, 1987; Desrochers et al., 2010; Copper et al., 2013). In contrast, overlying strata of the lowermost Becscie Formation, which records the Ordovician/Silurian boundary in the Anticosti Basin (e.g., Desrochers et al., 2010; Mauviel and Desrochers, 2016; Zimmt et al., 2024), are carbonate-dominated across the outcrop belt.

As one of the thickest and potentially best-preserved Ordovician/Silurian boundary sections in the world, the succession on Anticosti Island is a critical archive of paleobiological, paleoceanographic, and paleoclimatological data for understanding the sequence of Earth system events across the Ordovician/Silurian boundary. However, one of the main challenges in incorporating data from Anticosti into a global understanding of the Ordovician/Silurian boundary (e.g., Rong et al., 2020) has been the placement of the lower and upper bounds of the Hirnantian Stage within the succession (Riva, 1988; Brenchley et al., 1994; Melchin, 2008; Bergström et al., 2010, 2011, 2015; Jones et al., 2011; Achab et al., 2011, 2013; Mauviel and Desrochers, 2016; Zimmt and Jin, 2023). Much attention has been given to understanding the age of the Ellis Bay Formation; however, in contrast to the rest of the succession, the Ellis Bay Formation lacks abundant, diagnostic graptolites that could be used for graptolite-based age determination (though see Melchin, 2008). Much of the debate has focused on how to interpret the $\delta^{13}C$ record of the Ellis Bay Formation, and whether the formation records an expanded Hirnantian Carbon Isotope Excursion (HICE) with two distinct peaks (Mauviel and Desrochers, 2016), or instead the entirety of the $\delta^{13}C$ excursion is equivalent to what Mauviel and Desrochers (2016) referred to as the upper HICE (Bergström et al., 2010, 2011, 2015). Given the available biostratigraphic, chemostratigraphic, and sequence stratigraphic data from the Ellis Bay Formation, there are two plausible hypotheses for the age of the Western Ellis Bay Formation (usage following Copper et al., 2013).

The Hirnantian Stage on Anticosti Island is Restricted to the Uppermost Ellis Bay Formation

Support for this hypothesis is based primarily on carbon isotope chemostratigraphic and

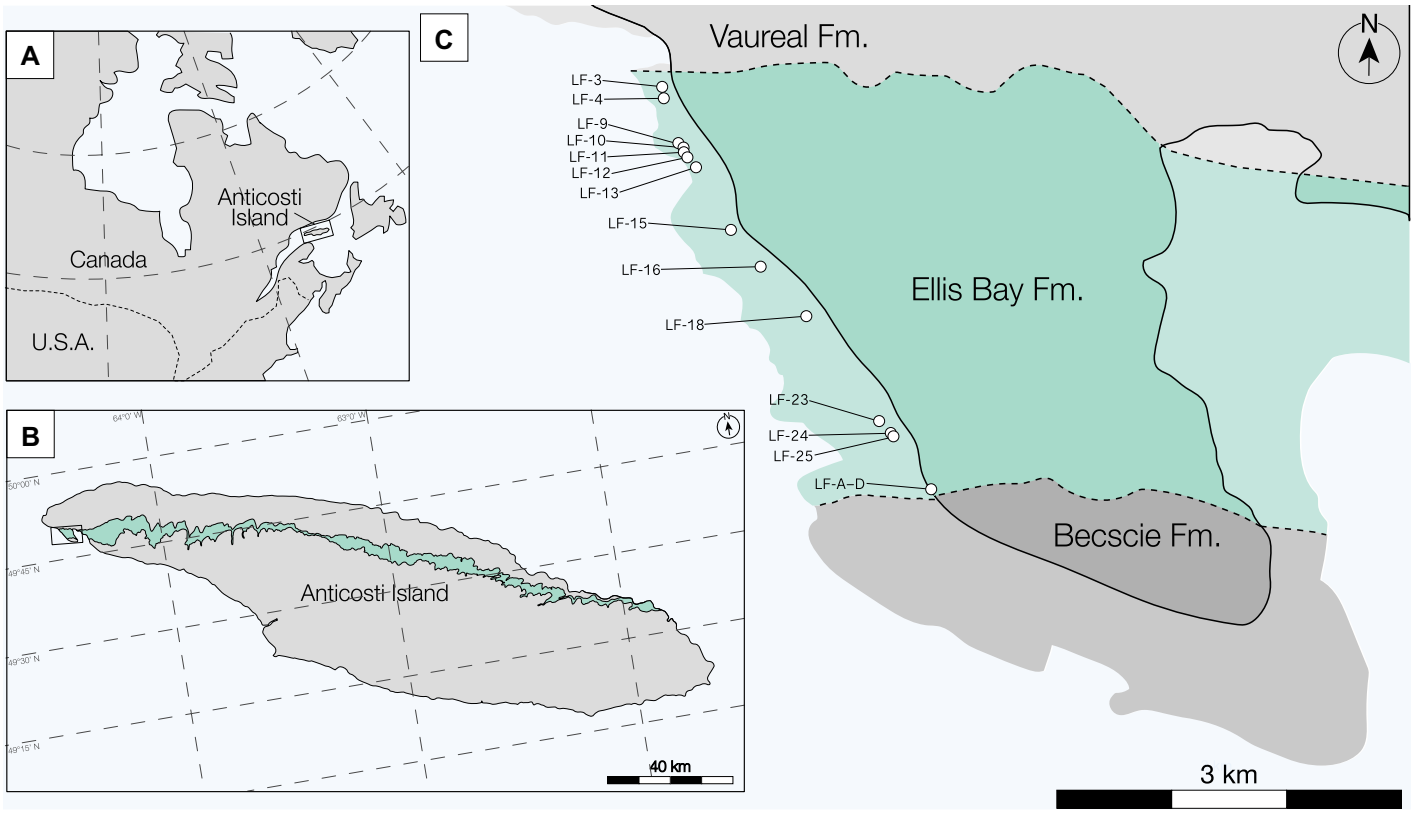

Figure 1. Regional and local context of the Western Ellis Bay Formation on Anticosti Island (Québec, Canada). (A) Location of Anticosti Island in eastern Canada (49°35′21″N, 63°02′54″W). (B) The mapped extent of the Ellis Bay Formation on Anticosti Island, shaded in green, with the study area on the western coast of the island outlined by a black box; map data from Desrochers and Gauthier (2009). (C) Location of sampling sites along the tidal bench of western Anticosti Island, where the bedrock of the island is exposed beyond the shoreline (solid black line) in a broad flat bench (lightly shaded area).

chitinozoan biostratigraphic correlation with Baltica. In Baltica, Porkuni (Hirnantian) strata comprise three chitinozoan zones that coincide with the HICE: the *Spinachitina taugourdeaui* (rising limb of the HICE), *Conochitina scabra* (peak values of the HICE, ~6‰–8‰), and barren zones (Brenchley et al., 1994, 2003; Kaljo et al., 2008; Hints et al., 2010). If these same zones are extrapolated to Anticosti Island, then the Hirnantian Stage in the Ellis Bay Formation would begin with the first occurrences of *S. taugourdeaui* and the rising limb of the upper HICE in the uppermost Lousy Cove Member; the lower HICE of Mauviel and Desrochers (2016) would correspond to one of the moderate- to low-magnitude carbon isotope excursions recorded by Katian strata in Baltica and Laurentia (Ainsaar et al., 2010; Bergström et al., 2010, 2020); this was the interpretation adopted by Finnegan et al. (2011). Incised valleys in the eastern Vaureal and Ellis Bay formations (Zimmt et al., 2024) would therefore have had to have formed prior to the Hirnantian, indicating eustatic fluctuations in the latest Katian (Calner et al., 2010; Turner et al., 2012; Ghienne et al., 2023). While muted, faunal turnover across the Vaureal/Ellis Bay contact (e.g., Bolton, 1981; Copper et al., 2013) would correspond to faunal turnover in the latest Katian, though this would post-date the pre-Hirnantian pulse of extinction that has been proposed by Rasmussen et al. (2019) based on an analysis of the global fossil record.

The Hirnantian Stage on Anticosti Island Comprises the Entirety of the Ellis Bay Formation

Support for this hypothesis comes from several different lines of evidence that indicate a major change in the Earth system occurred at the base of the Ellis Bay Formation. While bulk rock $\delta^{13}C$ values from the Ellis Bay Formation only reach higher values typical of the HICE in the Laframboise Member (4‰–5‰ Vienna Peedee belemnite [VPDB]; Fig. 2), there is considerable variability in the expression of the HICE among Hirnantian sections (Brenchley et al., 1994; Finney et al., 1999; Brenchley et al., 2003; Chen et al., 2006; Melchin and Holmden, 2006; Bergström et al., 2011, 2015; Mauviel and Desrochers, 2016; Ahm et al., 2017; Kiipli and Kiipli, 2020; Calner et al., 2021). Local processes strongly influence the expression of carbon isotope excursions in the geochemical record, even if the excursion itself reflects a response to changes in open ocean dissolved inorganic carbon (Melchin and Holmden, 2006; Swart, 2008; Ahm et al., 2017, 2018; Jones et al., 2020; Geyman and Maloof, 2021). In coeval Hirnantian sections around the world, multi-phased carbon isotope excursions are recorded by carbonate strata, including Monitor Range and Vinini Creek, Dobb's Linn, Arctic Canada, Estonia, and Mirny Creek (e.g., Underwood et al., 1997; Finney et al., 1999; Brenchley et al., 2003; Kaljo et al., 2004; Melchin and Holmden, 2006; Kaljo et al., 2012), supporting the plausibility of a two-phased HICE with an initial lower-magnitude excursion in the Anticosti Basin, as proposed by Mauviel and Desrochers (2016).

While sparse, the available graptolite record also indicates a Hirnantian age for the Western Ellis Bay Formation (Melchin, 2008), with members of the *Metabolograptus extraordinarius* and *M. persculptus* zones occurring below the base

of the Laframboise Member. A Hirnantian age for the entire Ellis Bay Formation is further supported by the first occurrences of the *Hirnantia* fauna at the base of the formation (Jin and Zhan, 2008; Copper et al., 2013; Copper and Jin, 2017; Zimmt et al., 2021; Zimmt and Jin, 2023): the migration of the *Hirnantia* fauna, a cool-water high-latitude fauna, to lower latitudes is used to mark the start of the Hirnantian Stage in tropical basins (Temple, 1965; Rong and Harper, 1988; Rong et al., 2020), reflecting a major shift in global climatic and oceanographic conditions as the Early Paleozoic Icehouse intensified (though see Rong et al., 2002). This episode of faunal turnover coincides with a pronounced change in stratigraphic architecture (Zimmt et al., 2024) and the development of a subaerial unconformity at the Vaureal/Ellis Bay contact, which has thus far been traced across the central and eastern parts of the island; the development of this unconformity has been attributed to the onset of larger glacio-eustatic fluctuations at the start of the Hirnantian Stage in response to a rapidly cooling climate (Desrochers et al., 2010; Zimmt et al., 2024).

METHODS

Sample Collection and Preparation

The only continuous section of the Western Ellis Bay Formation (sensu Copper et al., 2013) is preserved as a rocky tidal bench that extends several hundred meters beyond the shoreline of Anticosti Island; outcrops along the shoreline provide only intermittent exposures of the formation. Samples were collected from both this rocky tidal bench and outcrops along a transect from Anse aux Fraises to Pointe Laframboise (Fig. 1; 49°50′13.6″N, 64°27′11.5″W–49°48′06.6″N, 64°25′17.4″W); when possible, collections of fossils were made from micritic storm beds. The GPS coordinates of collections were used to project each sample into the stratigraphic section of Mauviel and Desrochers (2016), allowing for a direct comparison between our new fossil isotopic data and their bulk rock isotopic data. For this study, we used the revised stratigraphy of the Western Ellis Bay Formation from Copper et al. (2013), which established the current definitions of the Fraise, Juncliff, Parastro, Lousy Cove, and Laframboise members (though identical to the divisions of Copper, 2001) to subdivide the formation.

Rugose corals were selected as the primary sampling target for isotopic analysis, given their primary calcite mineralogy (Brand and Veizer, 1980) and abundance throughout the Ellis Bay Formation (Finnegan et al., 2011), providing the most complete stratigraphic coverage of all common carbonate fossil groups: in only two instances, brachiopods were used to supplement rugose coral data for stable isotope analyses. There has been some debate over the original magnesium content of rugose coral calcite, a factor that would impact ^{13}C–^{18}O reordering rates (Perez-Beltran et al., 2023). Available data suggest that rugose corals were highly sensitive to the Mg/Ca of seawater, precipitating low-Mg calcite under early Paleozoic calcite sea conditions and high-Mg calcite during late Paleozoic aragonite sea conditions (Brand and Veizer, 1980, 1981; Brand, 1981; Webb and Sorauf, 2002; Porter, 2010).

Fossils were sonicated in deionized water for half an hour to remove adhering sedimentary matrix. The epitheca (outer wall) of each coral was then removed by physical abrasion before the apex (initial portion of growth) of the coral was sampled using a rotating saw attached to a Dremel hand drill. Saw blades were operated at the lowest possible speed to prevent potential reordering effects during sample preparation; however, it is unknown whether rugose corals are similar to belemnites and more susceptible to reordering during drilling compared to other calcites (Staudigel et al., 2023). Coral apices were selected for sampling as they form prior to the development of septal insertions that can become occluded by marine sediment and late stage cements. Powdering entire apices yielded several 10^2s–10^3s mg of material from each coral for subsequent geochemical analyses. This amount of material is large enough that homogenized mixtures of multiple generations of carbonate cannot be ruled out. In some samples of colonial corals from the Laframboise Member, it was only possible to collect a piece of the coral from higher up on the corallite: visible infilling cement and sediments were removed using a Dremel hand drill, and then samples were sonicated in water once more. Rugose fragments and brachiopod flakes were selected and powdered using a mortar and pestle, following standard procedure (see Finnegan et al., 2011).

$\delta^{18}O$, $\delta^{13}C$, and Carbonate Clumped Isotope (Δ_{47}) Analysis and Data Reduction

Measurements of $\delta^{18}O$, $\delta^{13}C$, and Δ_{47} were carried out on 61 rugose corals at the Massachusetts Institute of Technology Carbonate Research Laboratory, Cambridge, Massachusetts, USA, following the methodology of Anderson et al. (2021), over the period from July 2020 to December 2021. Analysis was conducted on a Nu Perspective dual-inlet isotope ratio mass spectrometer, integrated with a Nu Carb automated sample preparation unit that was maintained at a temperature of 70 °C. Approximately 400–600 μg of calcite sample powder was weighed for each sample analysis. Samples were reacted with 150 μl of orthophosphoric acid, with a density of 1.94 g/cm^3, for 25 min to release CO_2 gas in individual glass vials. The evolved CO_2 gas was purified using cryogenic separation to remove water and other gases and further cleaned with a Porapak trap and silver wool, held at −30 °C.

The purified CO_2 gas, along with a reference gas of known composition, was measured using six Faraday collectors from 44 to 49, over three acquisitions each consisting of 20 cycles with a 20-second integration time, totaling 60 cycles and a 20 min overall integration time. The initial voltage setting was between 8 V and 20 V on the m/z 44 beam, with 2×10^8 Ω resistors. Across the analysis session, an ∼50% depletion in signal strength was observed, with sample and standard CO_2 gasses depleting at equivalent rates. Each analytical session, usually 50 individual analyses, started with the measurement of ETH-1–4 standards (Bernasconi et al., 2018, 2021) in a random order. This was followed by alternating blocks of three unknown samples and two ETH anchors, with additional standards like International Atomic Energy Agency (IAEA)-C1, IAEA-C2, and Merck measured once per run. This approach yields an unknown to standard ratio of 1:1. The standards ETH-1–4 and IAEA-C2 served as anchors, while other standards were treated as unknowns to maintain a balanced ratio of unknown to anchor samples. After every 10 analyses, the reference side of the dual-inlet system was replenished with reference gas to ensure consistency.

Raw mass spectrometer data were initially screened to remove cycles that deviated from more than 5 "long-term" standard deviations from the median Δ_{47} measurement. Analyses with significant cycle deviations, low transducer pressure, or reference-sample side depletion rate imbalances were excluded from further consideration. Details on excluded samples with low transducer pressure and depletion rate imbalances can be found in the Supplemental Material.[1] The "Δ_{47} crunch" Python package (Daëron, 2021), adhering to International Union of Pure and Applied Chemistry ^{17}O parameters, was then used for data processing, aligning raw Δ_{47} measurements with the I-CDES (InterCarb–

[1]Supplemental Material. Figures S1–S4, along with the full isotopic, trace element, and statistical datasets (Tables S1–S3). Please visit https://doi.org/10.1130/GSAB.S.29260196 to access the supplemental material; contact editing@geosociety.org with any questions.

Carbon Dioxide Equilibrium Scale) scale based on values from the InterCarb project (Bernasconi et al., 2021). A pooled-regression approach was applied for Δ_{47} conversion to I-CDES for error propagation that includes uncertainty in the I-CDES reference frame itself (Daëron, 2021). The long-term external repeatability of Δ_{47} across all analyses was determined to be 0.021‰ (1SD).

Additional measurements of $\delta^{18}O$ and $\delta^{13}C$ were carried out on 20 fossils at the Center for Stable Isotope Biogeochemistry at the University of California, Berkeley, California, USA, over the same period using a fully automated MultiCarb GV Isoprime system operated in Dual Inlet mode. These measurements were made to better understand the range in stable isotope values from targeted intervals within the Laframboise Member of the Ellis Bay Formation. All stable isotope values from both labs are reported relative to the VPDB standard; fluid equilibrium values are calculated from mineral $\delta^{18}O$ values and Δ_{47} temperatures using the supplemental equation from Anderson et al. (2021) for calcite-water equilibrium fractionation and are reported relative to Vienna Standard Mean Ocean Water (VSMOW). The full stable and carbonate clumped isotope dataset is available in the Supplemental Material.

Trace Element Analysis and μXRF Mapping

Of the 61 corals with Δ_{47} results, 55 were successfully analyzed for trace element concentrations using inductively coupled plasma–optical emission spectroscopy (ICP-OES). Measurements were performed by Activation Laboratories Ltd. (Actlabs, Ontario, Canada) on splits of the same powders used for Δ_{47} analysis. The protocol followed the Actlabs 1E3 method: samples were digested with Aqua regia with a 3:1 ratio of hydrochloric acid to nitric acid at 95 °C for 2 h before being diluted with deionized and ran using a Varian ICP-OES for 38 elements.

Of the 24 corals analyzed from the Laframboise Member, 14 were selected for additional micro-X-ray fluorescence (μXRF) mapping to examine the spatial variability of trace elemental concentrations across the coral, along with any infilling sediments or cement in between septa. To prepare samples for imaging, corals were cut along a transverse plane to produce thin disks that exposed the interior of each corallite. Disks were then embedded in Silmar-240 resin slabs and polished to provide a flat surface for imaging. Chemical imaging of fossils, as well as internal sediments and cements, was accomplished with a Bruker M4 Tornado benchtop μXRF spectrometer in the Division of Geological and Planetary Sciences Analytical Facility at Caltech, Pasadena, California, USA. X-rays were generated from a rhodium tube excited to 50 kV with 250 μA current. Samples in a 2-mbar vacuum were rastered beneath the primary X-ray beam, which was focused by polycapillary optics. Fluorescent X-ray energy spectra were measured simultaneously on two 30 mm^2 silicon drift energy dispersive spectrometer (EDS) detectors and assigned to 20-μm-wide pixels, which had primary beam dwell times of 20–40 ms per pixel. Bruker software (Bruker M4 Tornado v. 1.6) was used to deconvolve fluorescent X-ray EDS spectra from background, emission line overlaps, and detector artifacts (i.e., pile-up peaks and detector escape peaks).

RESULTS

Stratigraphic Patterns of $\delta^{13}C$ and $\delta^{18}O$ from the Ellis Bay Formation

Exposures of the uppermost Vaureal Formation in a rocky tidal bench along the western coast of Anticosti Island did not yield any well-preserved rugose corals that could provide a pre-Hirnantian reference frame for this analysis. Instead, we use data reported by Finnegan et al. (2011) from exposures of the Vaureal Formation across the western and central parts of the island to calculate a pre-Hirnantian reference frame for our mineral $\delta^{13}C$ and $\delta^{18}O$ datasets. Exposed strata of the Vaureal Formation in this half of the island are no more than ~0.5 m.y. older than the base of the Ellis Bay Formation (Long, 2007), providing a valuable point of comparison for our dataset. The 13 fossils from the Vaureal Formation reported by Finnegan et al. (2011) yield a mean ± σ $\delta^{13}C_{VPDB}$ of 0.2‰ ± 0.4‰ (n = 13) and a mean ± σ $\delta^{18}O_{VPDB}$ of −3.8‰ ± 0.5‰ (n = 13).

Carbon isotope values of rugose corals in the Western Ellis Bay Formation (Table S1) display a small positive $\delta^{13}C_{VPDB}$ increase (maximum = 3.0‰, mean ± σ = 2.5‰ ± 0.5‰; n = 16) in the Fraise Member (sensu Copper et al., 2013) when compared to available data from the Vaureal Formation (Fig. 2). A second, larger $\delta^{13}C_{VPDB}$ increase occurs within the Laframboise Member (maximum = 6.0‰, mean ± σ = 4.4‰ ± 0.8‰; n = 44); however, intervals within the Laframboise Member exhibit substantial $\delta^{13}C$ variability, of up to 3‰ (Fig. 3), exceeding the entire range of values recorded by the sub-Laframboise Ellis Bay Formation. Oxygen isotopes of rugose corals record a similar pattern: higher $\delta^{18}O_{VPDB}$ values (maximum = −2.0‰, mean ± σ = −2.4‰ ± 0.3‰; n = 16) toward the top of the Fraise Member when compared to the Vaureal reference frame (Fig. 2), followed by a large positive increase in the Laframboise Member (maximum = 1.7‰, mean ± σ = −1.7‰ ± 1.0‰; n = 44). As with $\delta^{13}C$, there is substantial variation in the $\delta^{18}O$ values of rugose corals within the Laframboise Member, with a range reaching ~4‰ within a single sampling interval (Figs. 3 and S1).

Fossils from the Ellis Bay Formation form two distinct populations in $\delta^{18}O$ versus $\delta^{13}C$ space. Fossils from the lower four members of the Ellis Bay Formation (sub-Laframboise) tend to have lower $\delta^{13}C$ and $\delta^{18}O$ values ($\delta^{13}C_{VPDB}$ mean ± σ = 2.0‰ ± 0.6‰; $\delta^{18}O_{VPDB}$ mean ± σ = −2.6‰ ± 0.3‰; n = 36) compared to the Laframboise Member ($\delta^{13}C_{VPDB}$ mean ± σ = 4.4‰ ± 0.8‰; $\delta^{18}O_{VPDB}$ mean ± σ = −1.7‰ ± 1.0‰; n = 44), with particularly strong differentiation in $\delta^{13}C$ (Fig. 4). Additionally, fossils from the Laframboise Member cover a greater range of both $\delta^{18}O$ and $\delta^{13}C$ values compared to those of the sub-Laframboise members. For this reason, we distinguish between samples from the sub-Laframboise Ellis Bay Formation and Laframboise Member throughout this manuscript.

Δ_{47} Temperatures and Reconstructed $\delta^{18}O_{water}$ from the Ellis Bay Formation

Clumped isotope (Δ_{47}) temperatures exhibit a relatively consistent range throughout the entire sub-Laframboise Ellis Bay Formation (minimum = 36 °C, mean ± σ = 42 ± 4 °C; n = 21; Fig. 2). Although the mean Δ_{47} temperature of Laframboise Member corals is similar to that of the sub-Laframboise Ellis Bay Formation, one population of values is substantially cooler, with nine samples below 35 °C (minimum = 28 °C, mean ± σ = 42 ± 11 °C; n = 24); however, Δ_{47} temperatures in this part of the formation can vary by up to 32 °C within a single ~0.3 m sampling interval (Fig. S1). Reconstructed equilibrium fluid $\delta^{18}O_{VSMOW}$ values vary considerably throughout the succession, with an increase in variability between the sub-Laframboise Ellis Bay Formation (mean ± σ = 1.5‰ ± 0.7‰; n = 21) and Laframboise Member (mean ± σ = 2.4‰ ± 1.4‰; n = 24).

Trace Elemental Analysis and μXRF Mapping

Analyzed specimens display substantial variability (order of 10^1–10^2 differences in concentration) in elements known to be sensitive to diagenetic processes, including Sr, Mg, Fe, and Mn (Fig. 5, Table S2). Significant positive covariation is observed between Sr and Mg ($R^2 = 0.24$, $p < 0.001$) and between Fe and Mn ($R^2 = 0.58$, $p < 0.001$) (Fig. S2; Table S3). Elemental mapping of 14 rugose corals from

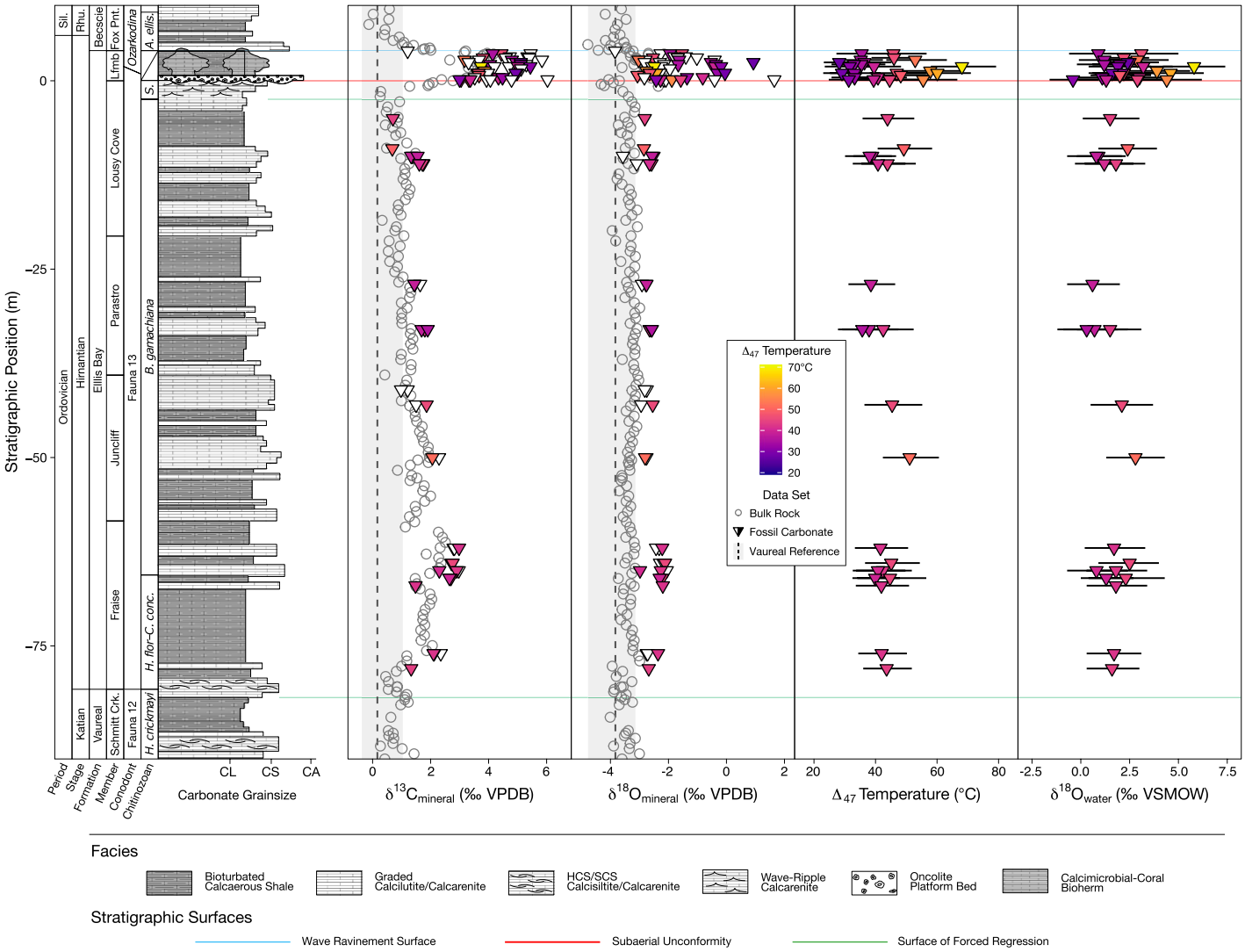

Figure 2. Fossil data from the Western Ellis Bay Formation plotted alongside bulk rock data from Mauviel and Desrochers (2016) and Mauviel et al. (2020); vertical dashed lines and light gray boxes indicate the mean and range, respectively, of fossil $\delta^{13}C$ and $\delta^{18}O$ values from the Vaureal Formation reported by Finnegan et al. (2011). Here, and in all figures, we assign a Hirnantian age to the entire Ellis Bay Formation and lowermost Becscie Formation. While both bulk rock and fossil isotopic data record concurrent intervals of increasing and decreasing fossil $\delta^{13}C$ and $\delta^{18}O$ values, bulk rock isotopic values are often lower than fossil data from the same stratigraphic interval. Δ_{47} temperatures are relatively consistent throughout the Ellis Bay Formation, except for the Laframboise Member (see Fig. 3). Lithostratigraphic data from Copper et al. (2013); conodont data from McCracken and Barnes (1981); chitinozoan data from Achab et al. (2011, 2013); stratigraphic column adapted from Mauviel et al. (2020). Sil.—Silurian; Rhu.—Rhuddanian; Lfmb—Laframboise Member; Fox Pnt.—Fox Point Member; *H. crickmayi*—*Hercochitina crickmayi*; *H. flor*—*Hercochitina florentini*; *C. conc.*—*Conochitina conica*; *B. gamachiana*—*Belonechitina gamachiana*; *S.*—*Spinachitina taugourdeaui*; *A. ellis.*—*Ancyrochitina ellisbayensis*; CL—calcilutite; CS—calcisiltite; CA—calcarenite; VPDB—Vienna Peedee belemnite; VSMOW—Vienna Standard Mean Ocean Water; HCS/SCS—hummocky and swaley cross-stratification.

the Laframboise Member demonstrates that coral septa and epitheca (outer wall) are consistently enriched in Sr relative to infilling cements and sediments, but the relationship of elements such as Fe and Mn between the coral and the infilling material is more complex (Fig. 6). In some specimens, coral skeletons contain less Fe and Mn than infilling sediment and cement, while in others the coral skeleton is enriched in Fe and Mn relative to the infilling cement. Additionally, the rims of corals collected from the lowest part of the Laframboise Member are often partially silicified, with silicification fronts moving inward toward the center of affected corals. Silicified areas of the coral contain high concentrations of Mg and Al, in contrast to areas that preserve the original carbonate mineralogy of the specimen.

DISCUSSION

Comparison of $\delta^{13}C$ and $\delta^{18}O$ Trends in Fossils and Bulk Rock Datasets

Both fossils (primarily rugose coral; this study) and bulk rock samples (Mauviel and Desrochers, 2016) record a two-phased positive $\delta^{13}C$ excursion within the Western Ellis Bay Forma-

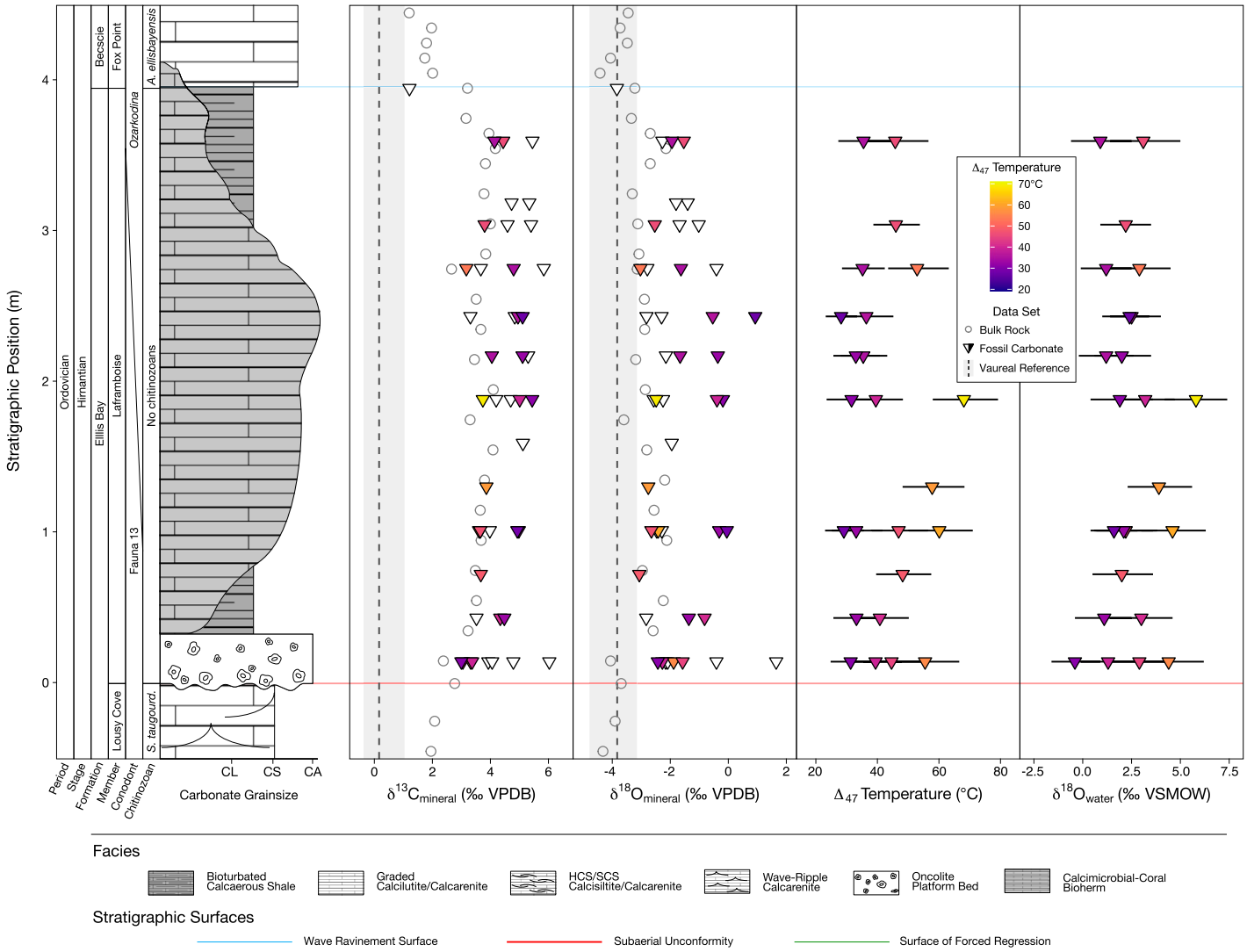

Figure 3. Fossil isotopic data from the Laframboise Member (see top of section in Fig. 2) of the Western Ellis Bay Formation plotted alongside bulk rock data from Mauviel and Desrochers (2016) and Mauviel et al. (2020); vertical dashed lines and light gray boxes indicate the mean and range, respectively, of fossil $\delta^{13}C$ and $\delta^{18}O$ values from the Vaureal Formation reported by Finnegan et al. (2011). While fossil $\delta^{13}C$ and $\delta^{18}O$ values both reach their maximum in the Laframboise Member, there is significant variability within each dataset, even within the same sampling interval. Δ_{47} temperatures present a similar pattern, reaching their minimum values within the Laframboise Member but with recorded temperatures ranging from 28.2 °C to 68.1 °C. Lithostratigraphic data from Copper et al. (2013); conodont data from McCracken and Barnes (1981) and Barnes (1988); and chitinozoan data from Achab et al. (2011, 2013). Stratigraphic column adapted from Mauviel et al. (2020). *A. ellisbayensis*—*Ancyrochitina ellisbayensis*; *S. taugourd*—*Spinachitina taugourdeaui*; CL—calcilutite; CS—calcisiltite; CA—calcarenite; VPDB—Vienna Peedee belemnite; VSMOW—Vienna Standard Mean Ocean Water; HCS/SCS—hummocky and swaley cross-stratification.

tion (Fig. 2). The magnitude of these excursions is larger in the fossil-derived dataset than in bulk rock data. In the fossil data, there is an initial positive $\delta^{13}C_{VPDB}$ excursion of 2.5‰–3.0‰ in the Fraise Member, versus 2.0‰–2.5‰ in the bulk rock data (termed the lower HICE by Mauviel and Desrochers, 2016), which returns to values close to the Vaureal reference frame by the top of the Lousy Cove Member. This is followed by a larger positive $\delta^{13}C_{VPDB}$ excursion of ~5.0‰ in corals from the Laframboise Member, versus ~4.0‰ in the bulk rock data (termed the upper HICE by Mauviel and Desrochers, 2016). Here, we find that rugose coral values within the peak of the upper HICE excursion are comparable (anywhere from 0‰ to 2‰ lower) to the peak values of the HICE recorded by fossils in other carbonate-dominated Hirnantian sections (e.g., Hints et al., 2010; Grossman and Joachimski, 2022).

Fossil (this study) and bulk rock (Mauviel et al., 2020) data record different trends in mineral $\delta^{18}O$ values throughout the Ellis Bay Formation despite their overlapping sampling intervals. In the fossil dataset, the upper Fraise Member records $\delta^{18}O_{VPDB}$ values 1.2‰–1.7‰ higher compared to fossils from the uppermost Vaureal Formation, representing a modest increase in $\delta^{18}O$ values that coincides with the lower HICE. In contrast, mineral $\delta^{18}O$ values from the bulk rock dataset do not record a notable increase in $\delta^{18}O$ values within the Fraise Member. A second interval with higher fossil $\delta^{18}O$ values

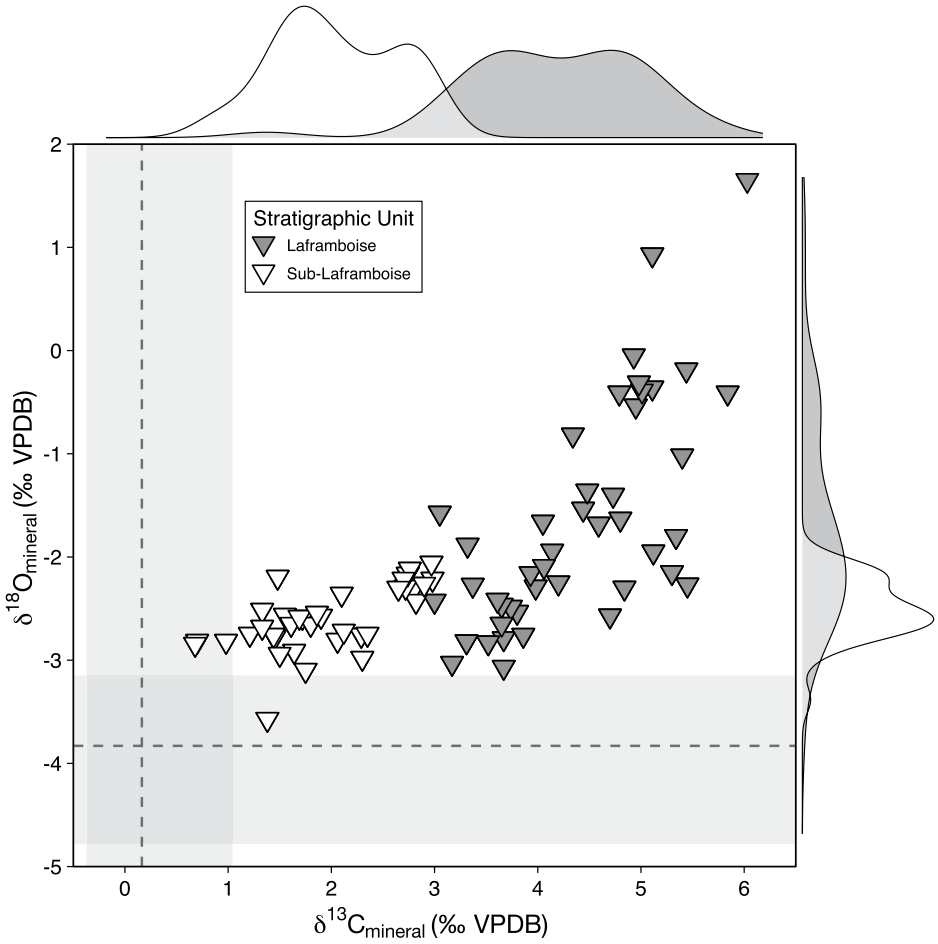

Figure 4. Comparison of fossil stable isotope data from the sub-Laframboise Ellis Bay Formation and Laframboise Member; vertical dashed lines and light gray boxes indicate the mean and range, respectively, of fossil $\delta^{13}C$ and $\delta^{18}O$ values from the Vaureal Formation reported by Finnegan et al. (2011). Probability density functions represent all fossils from a given stratigraphic interval. There is considerable separation of each array from the Ellis Bay Formation in $\delta^{13}C$ space, with minimal overlap between the two parts of the formation. In contrast, there is significant overlap in $\delta^{18}O$ space; however, the distribution of specimens from the Laframboise Member has a long positive tail, with half of all specimens from the member being higher than those from the sub-Laframboise Ellis Bay Formation. VPDB—Vienna Peedee belemnite.

occurs across the contact between the Lousy Cove and Laframboise members, coincident with the upper HICE. Here, the magnitude of the $\delta^{18}O_{VPDB}$ excursion (2.5‰–4.5‰) substantially exceeds the increase observed in bulk rock samples. Fossils from the Laframboise Member record $\delta^{18}O_{VPDB}$ values that are among the highest observed in Hirnantian fossils globally (0.0‰–1.7‰; Grossman and Joachimski, 2022). However, some rugose corals from the Laframboise Member have $\delta^{18}O$ values within the range of, or lower than, bulk rock from the same sampling interval (Figs. 2 and 3).

Increases in both fossil $\delta^{18}O$ and $\delta^{13}C$ values between the uppermost Vaureal and lowermost Ellis Bay formations coincide with turnover in marine benthic faunas (e.g., appearance of the *Hirnantia* fauna), as well as changes in stratigraphic architecture (e.g., development of incised valleys) and sedimentary facies (Copper, 2001; Jin and Zhan, 2008; Desrochers et al., 2010; Copper et al., 2013; Copper and Jin, 2017; Zimmt et al., 2024). Together, these coordinated changes strongly suggest a transition within the Anticosti Basin between the deposition of the Vaureal and Ellis Bay formations, similar to those observed across the Katian/Hirnantian boundary in Upper Ordovician sections around the world (e.g., Brenchley et al., 1994; Finney et al., 1999; Brenchley et al., 2003; Chen et al., 2006; Kaljo et al., 2008; Hints et al., 2010; Calner et al., 2021). On this basis, and the findings of previous work (see Geologic Background), we follow previous workers (e.g., Melchin, 2008; Desrochers et al., 2010; Copper et al., 2013; Mauviel et al., 2020; Zimmt and Jin, 2023) in ascribing a Hirnantian age to the entire Ellis Bay Formation.

Diagenetic Assessment of Fossils from the Ellis Bay Formation: Understanding the Preservation of $\delta^{13}C$, $\delta^{18}O$, and Δ_{47} Signatures

Estimating the Impact of Solid-State Reordering on Calculated Δ_{47} Temperatures from the Ellis Bay Formation

Constraining the extent of solid-state reordering experienced by fossils from the Ellis Bay Formation is critical for understanding the fidelity of our Δ_{47} temperature record as a signal of Hirnantian sea surface temperature change. At present, there is still uncertainty in the burial history of the Anticosti Basin, particularly regarding the amount of post-Silurian sediment cover that has since been removed. Accordingly, we calculate maximum estimates of solid-state reordering for fossils from the Ellis Bay Formation using single and double peak burial history models from Powell et al. (2018). Peak temperatures are estimated based on either the uppermost burial estimate from U-Th-He results (~2.3 km; Powell et al., 2018) or the maximum burial estimate from organic maturity data across Anticosti (3.2–3.5 km; Bertrand, 1990), both assuming a 26 °C/km geotherm. We note that neither represents the best estimate of burial history available from each study; instead, we use the maximum estimates to constrain the worst-case magnitude of Δ_{47} change due to solid-state reordering. When these maximum burial scenarios are combined with the reordering model of Hemingway and Henkes (2021), we find that the largest possible offset in calcite temperatures for fossils from the Ellis Bay Formation, due solely to solid-state reordering, would be 1.3 °C based on U-Th-He results or 7.1 °C based on organic maturity results (Fig. 7). We recognize, however, that a complete understanding of the factors that control the susceptibility of a carbonate sample to solid-state reordering, and quantifying them, remains a frontier in clumped isotope paleothermometry (Hemingway and Henkes, 2021; Li et al., 2021b; Looser et al., 2023; Lu et al., 2023; Perez-Beltran et al., 2023). Substitutions and defects in the crystal lattice can increase the rate of oxygen self-diffusion (Kronenberg et al., 1984); some fossils, including belemnites, have demonstrably higher reordering rates of ^{13}C–^{18}O bonds compared to optical calcite (Looser et al.,

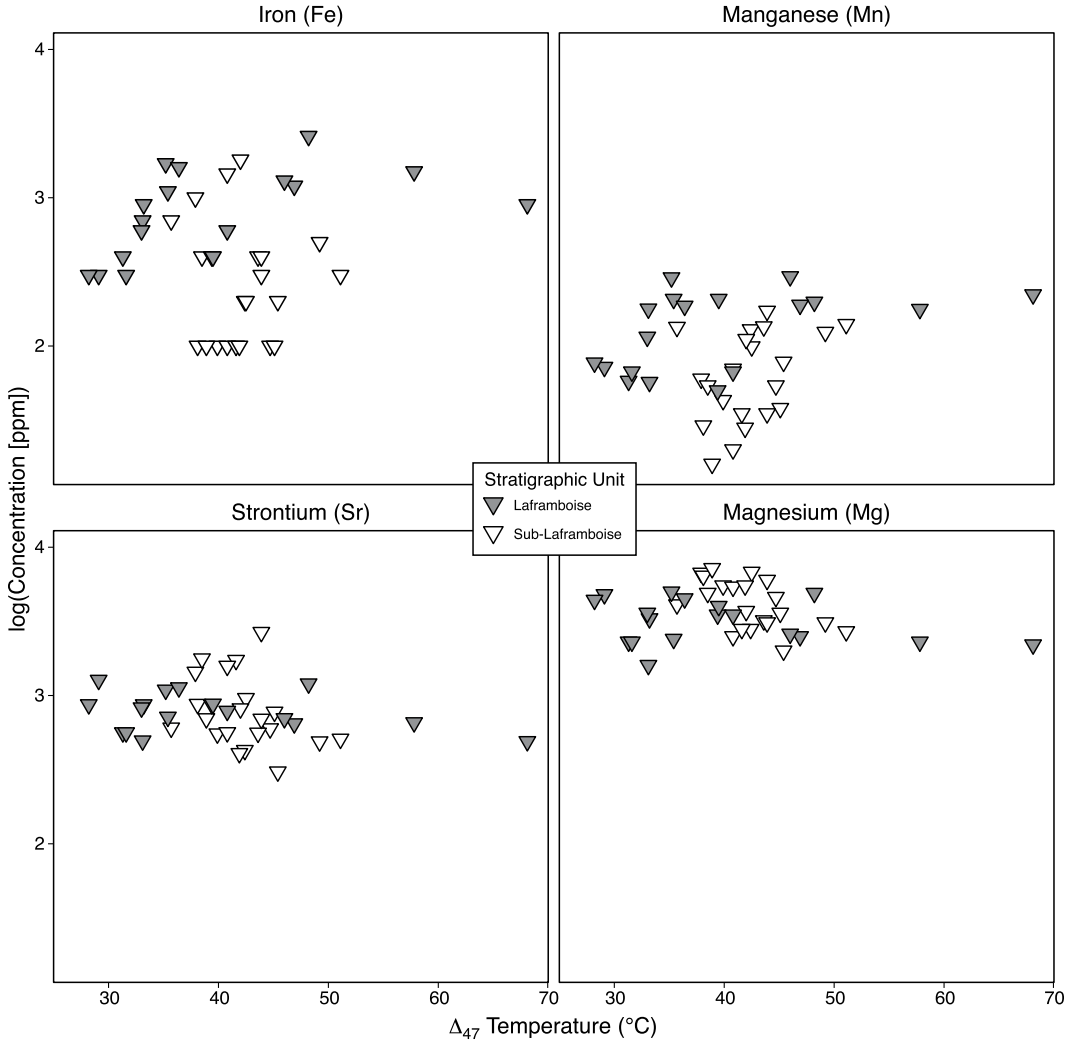

Figure 5. Log concentrations of diagenetically sensitive trace elements as a function of Δ_{47} temperature. When viewed in aggregate, corals from the Ellis Bay Formation show no relationship between trace element concentrations and Δ_{47} temperature; however, when separated into their respective stratigraphic intervals, specimens from the Laframboise Member (gray) display a positive correlation between Δ_{47} temperature and both log(Fe) and log(Mn), suggestive of diagenetic alteration in deep burial settings (Table S3; see text footnote 1); no correlation is observed between the concentration of trace elements and Δ_{47} temperature in the sub-Laframboise Ellis Bay Formation (white).

2023; Perez-Beltran et al., 2023). The range of Mg concentrations from our specimens (1600–7200 ppm) suggests that early Paleozoic rugose coral precipitated low-Mg calcite, as opposed to the range observed in high-Mg calcite (15,000–20,000 ppm) from late Paleozoic rugose corals (e.g., Brand and Veizer, 1981; Sorauf, 1997; Webb and Sorauf, 2002). Regardless, Ellis Bay corals are often characterized by higher concentrations of trace elements even when compared to Ordovician brachiopod fossils with a similar low-Mg calcite mineralogy (e.g., Brand and Veizer, 1980; Brand, 1981; Finnegan et al., 2011; Cummins et al., 2014). Experimental data on how these interactions influence solid-state reordering rates is limited: therefore, while our estimations of the extent of solid-state reordering represent an upper bound based on maximum burial scenarios, differences in reordering rates for early Paleozoic rugose corals could suggest that further modification of the Δ_{47} temperatures for fossils from the Ellis Bay Formation is indeed possible.

Sources of Secondary Variability in $\delta^{13}C$, $\delta^{18}O$, and Δ_{47} Values within the Ellis Bay Formation

Diagenetic alteration of biogenic calcite can be accompanied by a decrease in the concentration of Sr and increases in the concentrations of Mn and Fe, often also with corresponding decreases in the $\delta^{13}C$ and $\delta^{18}O$ values, as well as an increase in the Δ_{47} temperature, of a specimen (Brand and Veizer, 1980; Brand, 1983, 2004; Banner and Hanson, 1990; Shields et al., 2003; Finnegan et al., 2011; Ullmann and Korte, 2015; Bergmann et al., 2018; Lu et al., 2023). While no clear relationship can be found between the isotopic signature and trace element concentration of fossils from the lower Ellis Bay Formation (Figs. 5, S3, and S4; Table S3), samples from the Laframboise Member display a positive correlation between Δ_{47} temperature and Fe concentration expressed in ppm as log(Fe) ($R^2 = 0.27$, $p = 0.01$), as well as a weaker positive correlation with log(Mn) ($R^2 = 0.12$, $p = 0.08$); a negative correlation also exists between $\delta^{18}O$ and log(Fe) ($R^2 = 0.21$, $p = 0.03$). Bulk trace element results and μXRF data demonstrate that corals with the highest Δ_{47} temperatures in the Laframboise Member fall into two separate groups. The first consists of corals with relatively lower $\delta^{13}C$ and $\delta^{18}O$ values that are characterized by high concentrations of Fe and Mn in their skeletal calcite (Fig. 6). High Fe and Mn concentrations associated with the highest Δ_{47} temperatures are consistent with either the precipitation of secondary cements in the presence of anoxic burial fluids—where Δ_{47} powders represent a mixture of phases—or dissolution and reprecipitation of coral calcite during burial. The latter process, involving high water:rock ratio alteration, could have directly modified the elemental, $\delta^{18}O$, $\delta^{13}C$, and Δ_{47} signatures of the coral calcite (Brand and Veizer, 1980; Brand, 1983, 2004; Banner and Hanson, 1990; Finnegan et al., 2011; Looser et al., 2023; Lu et al., 2023). The second group of high Δ_{47} temperature corals has lower Fe and Mn trace element concentrations in the skeletal calcite, a

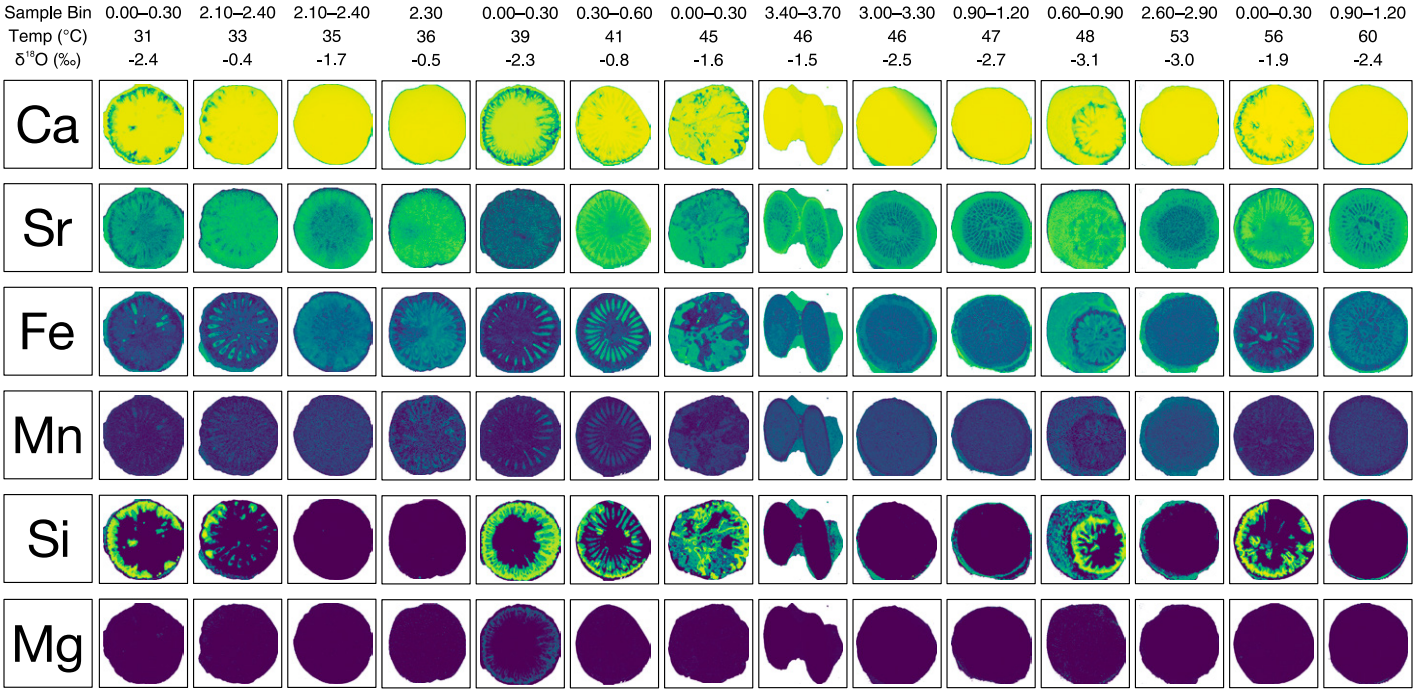

Figure 6. Elemental mapping of transverse sections of the apices of rugose corals from the Laframboise Member, arranged from lowest to highest clumped isotope temperature; sample bins refer to the stratigraphic intervals that were used to group samples during fieldwork. Intensity for each element is scaled to the maximum intensity for that element across all corals to enable a comparison between samples, with yellows corresponding to the highest and dark blues corresponding to the lowest intensities; all sample images have been rescaled to ensure that they can be viewed on the same panel. High-temperature corals with comparatively lower $\delta^{18}O$ values have calcite characterized by Fe and Mn enrichments, suggestive of high water:rock ratio alteration; high-temperature corals with higher $\delta^{18}O$ values possess trace element distributions more similar to that of well-preserved corals with lower Δ_{47} temperatures, suggestive of low water:rock ratio alteration (e.g., solid-state reordering, sediment-buffered alteration).

signature indicative of less alteration by anoxic fluids. Additionally, the calcite from these corals is characterized by higher concentrations of Sr and lower concentrations of Fe and Mn relative to infilling cements and sediments (Fig. 6), and $\delta^{13}C$ and $\delta^{18}O$ values similar to low-temperature corals, consistent with alteration under low water:rock ratio conditions (Brand and Veizer, 1980; Brand, 1983, 2004).

When plotted in a three-dimensional space, comprising $\delta^{18}O_{VPDB}$, Δ_{47} temperature, and reconstructed $\delta^{18}O_{VSMOW}$ of water (e.g., Eiler, 2011; Bergmann et al., 2018; Goldberg et al., 2021), the data from fossils of both the sub-Laframboise Ellis Bay Formation and Laframboise Member reflect this same combination of diagenetic processes (Fig. 8), with fossils from the Laframboise Member showing a stronger influence of high water:rock ratio alteration. Grouping data from the Laframboise Member by sampling interval provides a clearer picture of how diagenetic pathways contributed to the range of $\delta^{13}C$, $\delta^{18}O$, and Δ_{47} temperatures in this part of the formation (Fig. S1). Measured $\delta^{18}O_{VPDB}$ values within individual sampling intervals from the Laframboise Member, ranging up to ~4‰, are consistent with variable water:rock ratio alteration in the presence of marine fluids. Sampling included both bioherms and muddy intermound fill, which were subsequently grouped as the same horizon while in the field: this sampling approach may have contributed to the observed isotopic variability and differences in diagenetic pathways. Similarly, the differences in Δ_{47} temperatures within sampling intervals, ranging from 10 °C to 36 °C (corresponding to differences in calculated $\delta^{18}O_{VSMOW}$ ranging from 1.0‰ to 4.8‰) are attributed to variable water:rock ratio alteration, with one endmember characterized by sediment-buffered diagenesis rather than solely solid-state reordering.

Consideration of Diagenetic Influences on the Final Isotopic Record of the Ellis Bay Formation

Fossils that experienced predominantly low water:rock ratios (e.g., through sediment-buffered diagenesis) are more likely to retain more primary isotopic signatures like $\delta^{13}C$ and $\delta^{18}O$ compared to those that interacted with high water:rock ratios in the burial environments, although Δ_{47} temperatures are independently sensitive to peak burial temperature (e.g., Bergmann et al., 2018; Goldberg et al., 2021). Specimens more affected by open-system alteration tend to be characterized by higher concentrations of Fe and Mn (Figs. 5 and 6), and by $\delta^{18}O$ and $\delta^{13}C$ values that plot within the range of values from the surrounding bulk rock (Figs. 2 and 3). To minimize the effects of open-system alteration in our analysis of Hirnantian seawater changes within the Anticosti Basin, we adopt the criteria used by Barney and Grossman (2022) for Katian brachiopods, considering rugose coral samples with Fe >400 ppm and Mn >150 ppm to be highly altered (Fig. 5). For the 26 specimens from the Laframboise Member lacking trace element data, we classify them as altered if they (1) have lower isotopic values compared to well-preserved fossils from the same sampling interval, and (2) fall within the $\delta^{13}C$ and $\delta^{18}O$ range of bulk rock from the same sampling interval, in contrast to well-preserved samples from the Laframboise Member (Figs. 3 and S1). Applying these criteria produces coherent isotopic profiles for the entire Ellis Bay Formation (Figs. 9 and 10; compared to Figs. 2 and 3).

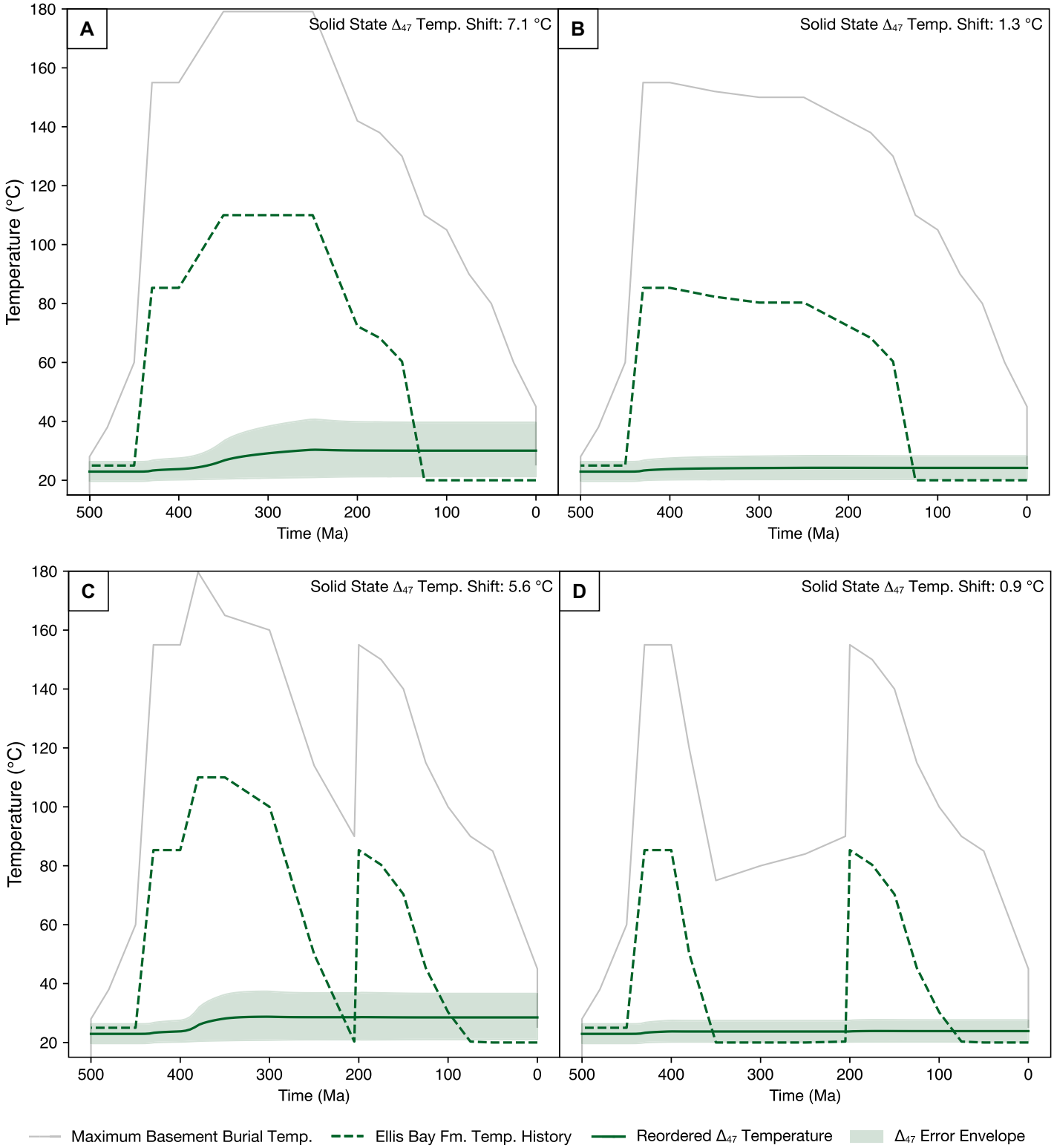

Figure 7. Estimates of the influence of solid-state reordering on the Δ_{47} temperature of fossils from the Ellis Bay Formation, combining the solid-state reordering model of Hemingway and Henkes (2021) with the two burial history models (A and B, compared to C and D) for the Ellis Bay Formation proposed by Powell et al. (2018). Temperature histories for the Ellis Bay Formation are calculated based on the maximum amount of post-Silurian cover estimated by Bertrand (1990; A, C) or by Powell et al. (2018; B, D), the thermal gradient calculated by Powell et al. (2018), and the position of the Ellis Bay Formation relative to the basement from Long (2007).

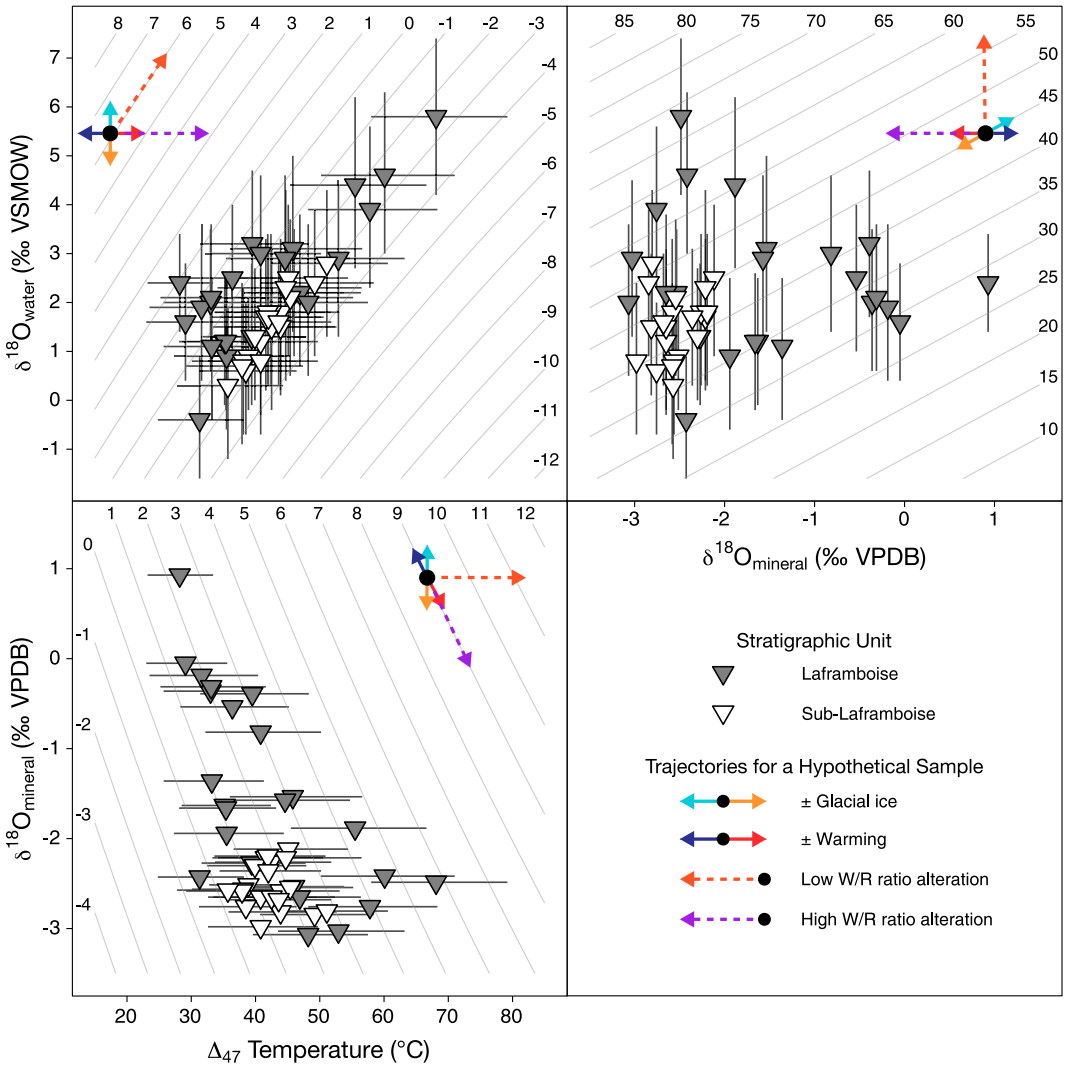

Figure 8. Distribution of samples in a three-dimensional space composed of $\delta^{18}O_{VPDB}$, Δ_{47} temperature, and reconstructed $\delta^{18}O_{VSMOW}$ of water following Bergmann et al. (2018); gray lines are contours of the third, unplotted value in each two-dimensional plot. Trajectories indicated in each plot reflect the response of a specimen to different primary and secondary processes. In each plot, the distribution of samples from both the sub-Laframboise Ellis Bay Formation (white) and Laframboise Member (gray) reflects the variable influence of low and high water:rock (W/R) ratio alteration; samples from the Laframboise Member show a comparatively large range in isotopic values, suggesting greater variation in both primary values and secondary diagenetic processes. VPDB—Vienna Peedee belemnite; VSMOW—Vienna Standard Mean Ocean Water.

The Significance of the Ellis Bay Formation as a Record of Hirnantian Climate Change

Placing Δ_{47} Temperature and $\delta^{18}O$ Data from the Ellis Bay Formation in a Global Context

Daëron and Vermeesch (2024) recently compared the Δ_{47} temperature calibration of Anderson et al. (2021), used in this study, to other Δ_{47} temperature calibrations within the I-CDES reference frame. They found that calculated Δ_{47} temperatures were statistically indistinguishable among the studied calibrations, with differences of 0.5 °C or less between the combined calibration equation and the regression published in Anderson et al. (2021) for Δ_{47} values <50 °C. This gives us some confidence in the accuracy and repeatability of our calculated Δ_{47} temperatures. However, caution is warranted when comparing our Δ_{47} temperatures to the results from other recent carbonate clumped isotope studies. The inter-laboratory comparison project by Bernasconi et al. (2021) suggests that inter-laboratory differences are amplified by differences in data processing methods (e.g., using in-house heated and equilibrated gases for correction to the CDES reference frame instead of using ETH standards and the I-CDES reference frame; omitting a pressure baseline correction in the presence of an instrument-specific δ^{47}-dependence; or applying a Δ_{47} calibration based on a reference frame distinct from I-CDES). Based on the results from Bernasconi et al. (2018, 2021), we estimate that these choices may lead to differences as large as 5–10 °C for Δ_{47} values <50 °C.

A recent study of Katian brachiopods from Laurentia (Barney and Grossman, 2022) published Δ_{47} temperatures using the CDES reference frame of Dennis et al. (2011) and a calibration based on ETH standard values published prior to the publication of the I-CDES reference frame. Transforming samples into the I-CDES reference frame with the ETH standards run alongside the samples and using the Anderson et al. (2021) calibration shifts the sample population from 25 °C to 55 °C (mean $\pm\sigma$ = 36 ± 7 °C; n = 28) to 24–72 °C (mean $\pm\sigma$ = 40 ± 11 °C; n = 28), with only two samples with Δ_{47} temperatures cooler than 28 °C. Thus, when data processing steps are equivalent, our final dataset (minimum = 28 °C, mean $\pm\sigma$ = 40 ± 6 °C; n = 21) and the recalculated dataset from Barney and Grossman (2022) have similar distributions and means. Thiagarajan et al. (2024) published a Δ_{47} dataset based on brachiopods and well-preserved micrites from Baltica, with calculated Δ_{47} temperatures ranging from 23 °C to 61 °C. While this distribution is consistent with latitudinal temperature variability, as Baltica migrated from higher latitudes to the tropics over the course of the Ordovician (e.g., Torsvik and Cocks, 2016; Cocks and Torsvik, 2021; Judd et al., 2024), these results cannot immediately be compared to the present study because Thiagarajan et al. (2024) used an approach for their data processing and calibration that did not rely on ETH standards: more

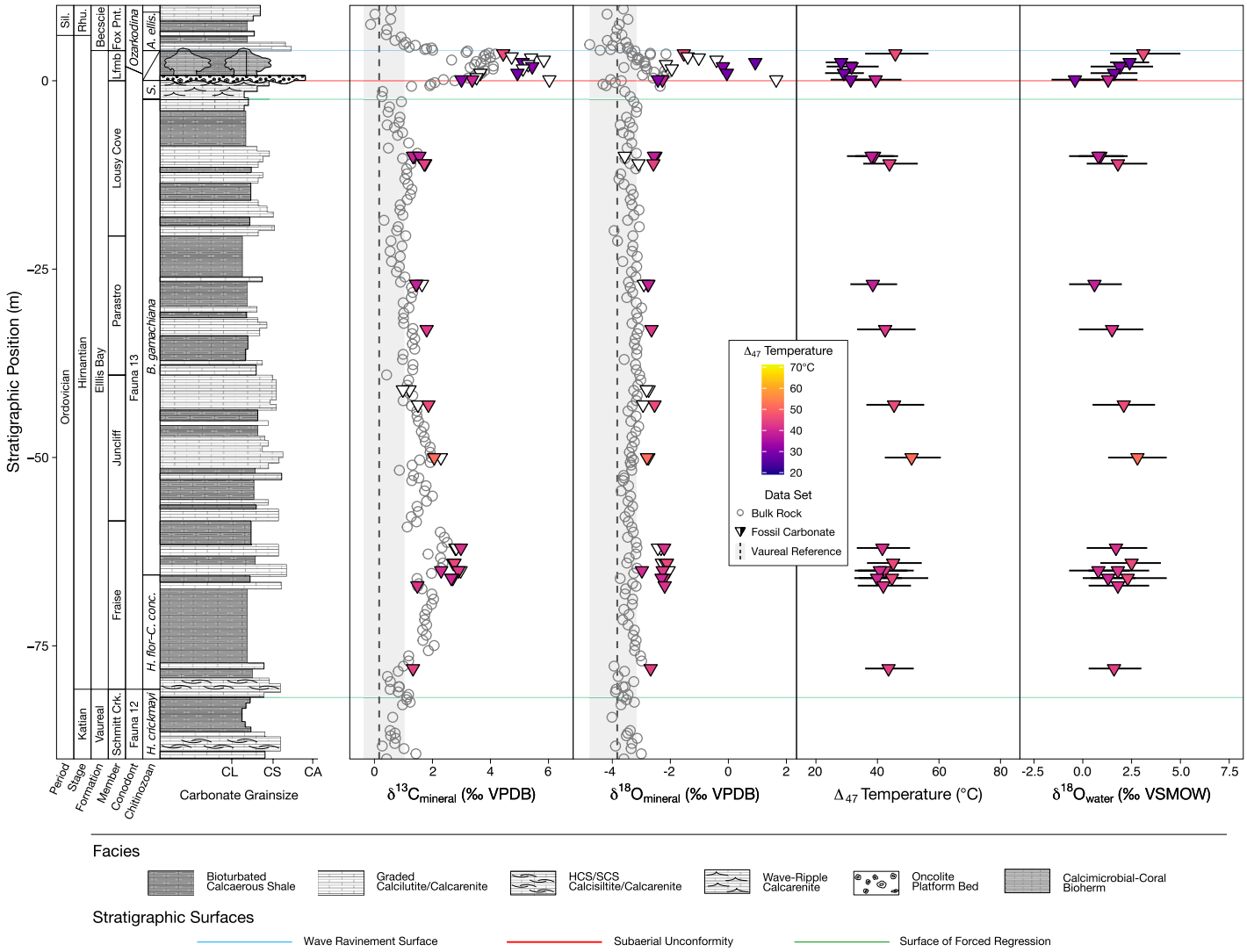

Figure 9. Final isotopic dataset for the entire Ellis Bay Formation, as in Figure 2, but now with only well-preserved fossil samples plotted for each sampling interval. Vertical dashed lines and light gray boxes indicate the mean and range, respectively, of fossil $\delta^{13}C$ and $\delta^{18}O$ values from the Vaureal Formation reported by Finnegan et al. (2011). Scatter in both stable and carbonate clumped isotope space has been reduced throughout the formation, most notably in the Laframboise Member (Fig. 10). Sil.—Silurian; Rhu.—Rhuddanian; Lfmb—Laframboise Member; Fox Pnt.—Fox Point Member; *H. crickmayi*—*Hercochitina crickmayi*; *H. flor*—*Hercochitina florentini*; *C. conc.*—*Conochitina conica*; *B. gamachiana*—*Belonechitina gamachiana*; *S.*—*Spinachitina taugourdeaui*; *A. ellis.*—*Ancyrochitina ellisbayensis*; CL—calcilutite; CS—calcisiltite; CA—calcarenite; VPDB—Vienna Peedee belemnite; VSMOW—Vienna Standard Mean Ocean Water; HCS/SCS—hummocky and swaley cross-stratification.

data and work are needed to properly make such a comparison (see Grossman et al., 2025). Additionally, as noted by Bergmann et al. (2025) and Grossman et al. (2025), the very cold Hirnantian equatorial temperatures predicted by Thiagarajan et al.'s (2024) model are well below those observed in any Cenozoic analog state.

In light of the complications posed by both diagenesis and inter-laboratory differences in the processing of Δ_{47} data, comparison of mineral $\delta^{18}O$ values may be more immediately informative for understanding climate change throughout the Late Ordovician. Published brachiopod $\delta^{18}O_{VPDB}$ values from Barney and Grossman (2022) range from −5.27‰ to −2.57‰ (mean ± σ = −4.64‰ ± 0.58‰; n = 28), with only the highest isotopic values overlapping with the range in $\delta^{18}O_{VPDB}$ values from the Ellis Bay Formation. Similarly, brachiopod $\delta^{18}O_{VPDB}$ values reported by Thiagarajan et al. (2024) range from −6.91‰ to −3.60‰ (mean ± σ = −5.19‰ ± 0.80‰; n = 23). In contrast, fossil $\delta^{18}O_{VPDB}$ values from our screened Ellis Bay dataset are notably higher, ranging from −3.57‰ to 1.65‰ (mean ± σ = −2.08‰ ± 1.08‰; n = 40). If we expand this comparison to include isotopic data from tropical Ordovician/Silurian boundary sections around the world, we find that fossils from the Laframboise Member have equivalent or higher $\delta^{18}O$ values, but lower $\delta^{13}C$ values, relative to other Hirnantian sections (Fig. 11). Fossils from the sub-Laframboise Ellis Bay Formation occupy a unique region in isotopic space between Katian and Hirnantian samples, with the highest $\delta^{18}O$ and $\delta^{13}C$ values corresponding to the interval of the lower HICE (Fig. 9). Fossil $\delta^{18}O$ values from the Ellis Bay Formation are thus consistent with an intensifying icehouse

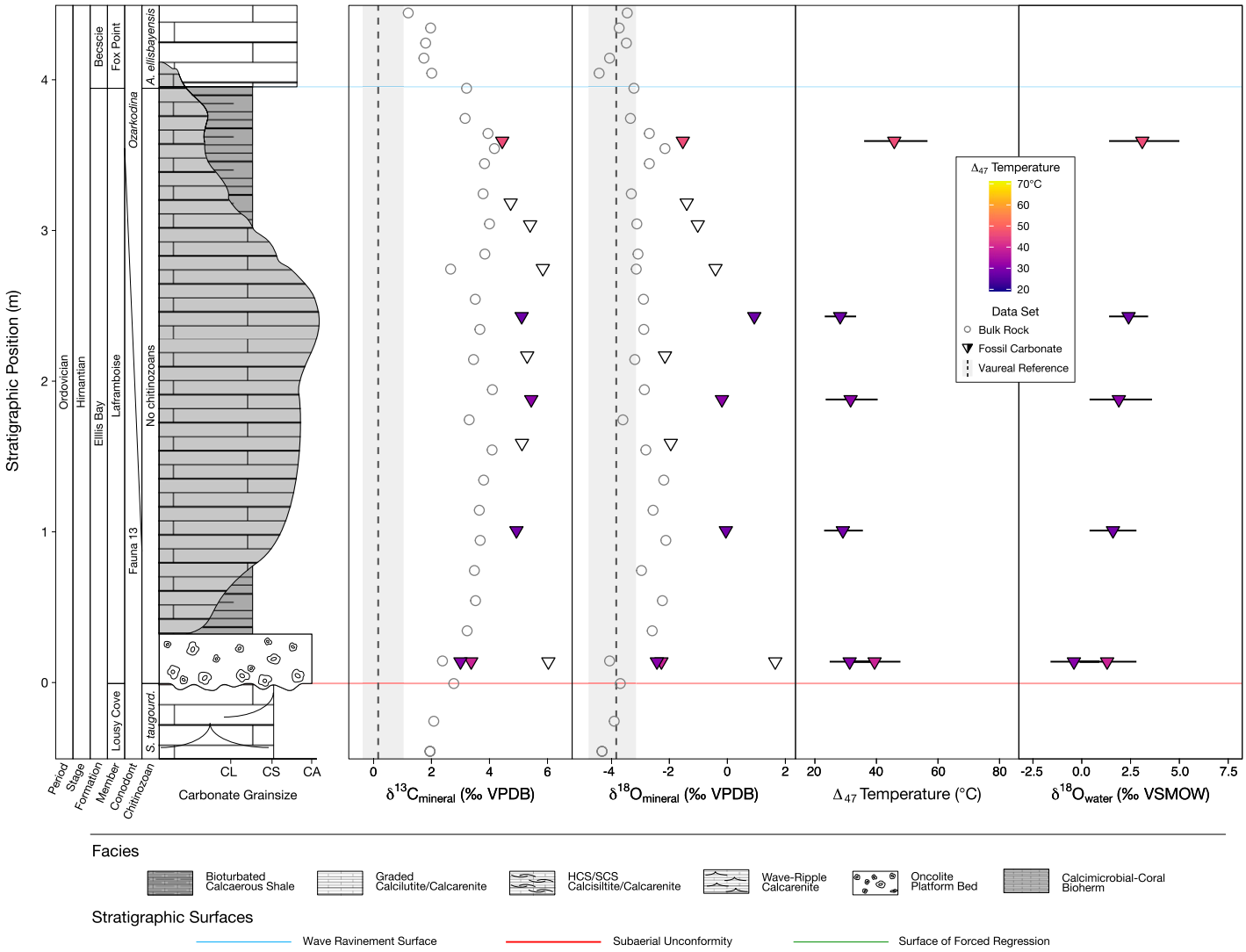

Figure 10. Final isotopic dataset for the Laframboise Member, as in Figure 3, but now with only well-preserved fossil samples plotted for each sampling interval. Vertical dashed lines and light gray boxes indicate the mean and range, respectively, of fossil $\delta^{13}C$ and $\delta^{18}O$ values from the Vaureal Formation reported by Finnegan et al. (2011). Excluded samples with higher Δ_{47} temperatures and lower $\delta^{18}O$ values most often plot within the range of values recorded by bulk rock, suggesting that bulk rock and the excluded samples (fossil carbonate) experienced similar alteration processes. The remaining well-preserved samples record a plateau in $\delta^{13}C$ and $\delta^{18}O$ values throughout the Laframboise Member; $\delta^{18}O$ values begin to decrease within the upper meter of the member, coinciding with a gradual increase in recorded Δ_{47} temperatures. *A. ellisbayensis*—*Ancyrochitina ellisbayensis*; *S. taugourd*—*Spinachitina taugourdeaui*; CL—calcilutite; CS—calcisiltite; CA—calcarenite; VPDB—Vienna Peedee belemnite; VSMOW—Vienna Standard Mean Ocean Water; HCS/SCS—hummocky and swaley cross-stratification.

during the Hirnantian Stage, recording evidence of increasing continental ice mass and cooling tropical sea surface temperatures, even where arguments based on Δ_{47} temperature alone are less straightforward and masked by alteration.

The number of other high-resolution, stratigraphically constrained, and well-preserved Hirnantian fossil $\delta^{18}O$ datasets comparable to the current study is, at present, limited. Available datasets from Baltica capture two distinct phases of increasing $\delta^{18}O$ in the Late Ordovician, the first at the Katian/Hirnantian boundary and the second in the middle to late Hirnantian (Brenchley et al., 1994; Hints et al., 2010). Each of these phases of increasing fossil $\delta^{18}O$ has a magnitude of 1.5‰–3.0‰, a similar pattern to the Ellis Bay Formation that would suggest that both the Anticosti Basin and Baltica record a similar response to global climate change during the Hirnantian Stage. Importantly, we note that no persistent, positive $\delta^{18}O$ excursions of a similar magnitude (1.5‰–3.0‰) have been documented in Katian fossil $\delta^{18}O$ records (e.g., Goldberg et al., 2021; Barney and Grossman, 2022).

The Hirnantian Glacial Maximum in the Anticosti Basin: Implications for Understanding the Late Ordovician Mass Extinction

The Hirnantian Glacial Maximum, representing the most intense glacial episode of the early Paleozoic, has long been thought to play a critical role in causing the Late Ordovician mass extinction. Throughout the Upper Ordovician to lower Silurian succession on Anticosti Island, the largest recorded increase in fossil and bulk rock carbonate $\delta^{18}O$ values occurs at the con-

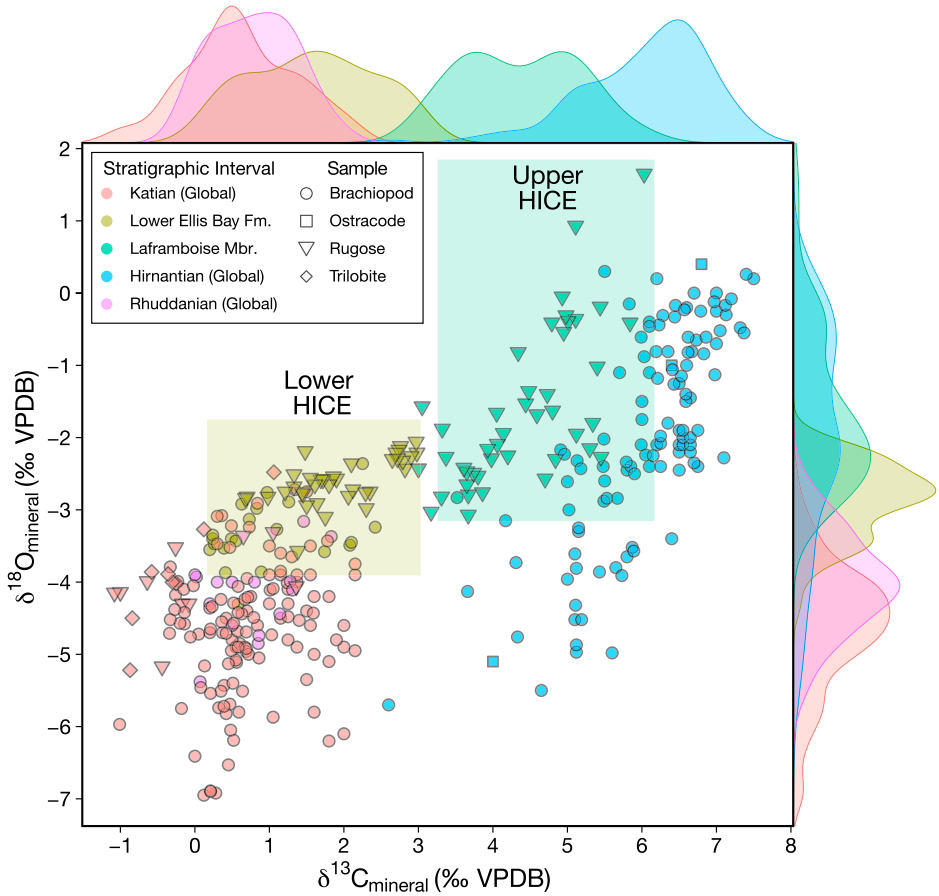

Figure 11. Comparison of fossil stable isotope data from Ordovician/Silurian boundary sections around the world published in Grossman and Joachimski (2022), supplemented with data from the present study, as well as Brenchley et al. (1994) and Hints et al. (2010). Global data do not include the Ellis Bay Formation; data from the Western Ellis Bay Formation are broken into the lower Ellis Bay Formation (i.e., interval recording the lower Hirnantian Isotopic Carbon Excursion [HICE]) and the Laframboise Member (i.e., interval recording the upper HICE). Probability density functions represent all fossils from a given stratigraphic interval. Here, we note that the well-preserved samples plotted in Figures 9 and 10 tend to plot at the upper end of their respective density distributions. The lower Ellis Bay Formation occupies a transitional space between fossils from Katian strata and fossils from the Laframboise Member and Hirnantian strata globally: this effect is most pronounced in $\delta^{18}O$ space. VPDB—Vienna Peedee belemnite.

tact between the Lousy Cove and Laframboise members (Mauviel and Desrochers, 2016); this excursion is accompanied by an ~10 °C drop in the best-preserved fossil Δ_{47} temperatures, signaling a major cooling of tropical oceans (Figs. 9 and 10). Fossils from the Laframboise Member record some of the highest $\delta^{18}O$ values from Hirnantian strata globally (Fig. 11). Together, these observations suggest the Laframboise Member records evidence for substantial tropical cooling and expansion of Gondwanan ice sheets compared to conditions recorded in the lower Ellis Bay Formation.

Stratigraphic evidence clearly points toward an intensification of the icehouse climate in the uppermost Lousy Cove Member. Sequence stratigraphic models predict that the intensification of icehouse climate conditions should cause the development of a regressive surface of marine erosion and subaerial unconformity in the stratigraphic record through glacio-eustatic forcing (Hunt and Tucker, 1992; Zecchin and Catuneanu, 2013), with subaerial erosion removing strata and fossils from below the unconformity that would have otherwise have recorded cooling temperatures and increasing $\delta^{18}O$ values leading up to the glacial maximum. In the uppermost Lousy Cove Member, a sharply defined regressive surface of marine erosion marks the transition from lime mudstone to wave-rippled calcarenite, signaling glacial advance and sea-level fall (Figs. 9 and 10; Desrochers et al., 2010; Zimmt et al., 2024). Above this surface at the Lousy Cove/Laframboise contact, physical stratigraphic evidence indicates a prolonged period of subaerial weathering and erosion (Desrochers et al., 2010; Ghienne et al., 2014; Zimmt et al., 2024). An abrupt shift in both stable and clumped isotope values across this contact, consistent with glacial advance and significant tropical cooling (Figs. 9 and 10), supports the interpretation that this erosional surface marks the Hirnantian Glacial Maximum in the Anticosti Basin. While the Laframboise Member itself was previously considered to represent the Hirnantian Glacial Maximum (Copper, 2001; Finnegan et al., 2011), we argue that it is more properly considered to reflect conditions that post-date the peak of the icehouse, which is instead represented by evidence of sea-level fall and subaerial weathering and erosion at the underlying unconformity. Nonetheless, the Laframboise Member was likely deposited while there was still a substantial volume of ice on Gondwana.

Along the Western Coast of Anticosti Island, facies shifts in the Laframboise Member reflect a gradual increase in water depth. Gradually decreasing $\delta^{18}O$ values, concurrent with rising Δ_{47} temperatures throughout the member (Fig. 10) are both consistent with sea surface warming and deglacial sea level rise. This signal is abruptly truncated at the contact between the Laframboise Member and the overlying Fox Point Member of the Becscie Formation, with a rapid return to pre-Hirnantian $\delta^{18}O$ and $\delta^{13}C$ values. Physical stratigraphic evidence indicates that this contact is a pronounced transgressive ravinement surface, marked by a well-developed hardground, the drowning of the Laframboise bioherms, and a sharp shift from inner ramp (Laframboise Member) to deep-subtidal facies (Fox Point Member), reflecting the abrupt flooding of the ramp (Desrochers et al., 2010; Jones et al., 2011; Copper and Jin, 2014; Ghienne et al., 2014; Zimmt et al., 2024). Bioherm development in the Laframboise Member following the peak of glaciation, culminating in a drowning event and the development of a hardground, resembles records preserving Holocene Meltwater Pulse 1A, highlighting how abrupt early deglacial eustatic sea-level rise can dramatically reshape carbonate ramp ecosystems (Fairbanks, 1989; Cronin, 2012; Blanchon and Chutcharavan, 2023).

In summary, both stratigraphic and geochemical evidence in the Anticosti Basin suggest that ice sheet growth began at the contact between the Vaureal and Ellis Bay formations (Katian/Hirnantian boundary), preceding a pronounced

increase in ice volume at the contact between the Lousy Cove and Laframboise members, marking the Hirnantian Glacial Maximum (middle to late Hirnantian). Given that the true peak of the icehouse is represented by the unconformity at the Lousy Cove/Laframboise contact, the preserved $\delta^{18}O$ increase at this surface (2.5‰–4.5‰ in fossil $\delta^{18}O_{VPDB}$) only serves as a lower constraint on the combined effect of increasing continental ice mass and tropical sea surface cooling during the peak of the Early Paleozoic Icehouse. Regardless, the total $\delta^{18}O_{VPDB}$ increase of ~4‰–5‰ between the Vaureal and Ellis Bay formations is comparable to tropical $\delta^{18}O$ excursions associated with glacial advances during the Late Paleozoic Icehouse (Grossman et al., 2008). While caution is warranted in the interpretation of epicontinental isotope records (e.g., Swart, 2008; Grossman et al., 2008; Ahm et al., 2017; Judd et al., 2020), the magnitude of this excursion suggests that the Early Paleozoic Icehouse may have had an impact on the Earth system comparable to or exceeding subsequent icehouse climates.

Our study thus substantially revises the only previous paired $\delta^{18}O$ and Δ_{47} assessment of the Ordovician/Silurian boundary by Finnegan et al. (2011), which regarded the Laframboise Member as a representative Hirnantian section that captured the full range of isotopic variability throughout the Hirnantian Glacial Maximum. The Δ_{47} temperature and mineral $\delta^{18}O$ curves presented in Finnegan et al. (2011) are here interpreted to only capture a small subset of Hirnantian climate and oceanographic change following the peak of the Early Paleozoic Icehouse. Conclusions based on the findings of Finnegan et al. (2011; e.g., Melchin et al., 2013; Rohrssen et al., 2013; Jones et al., 2017; Bond and Grasby, 2020; Longman et al., 2021; Rasmussen et al., 2023) should therefore be revised accordingly, particularly given that in the Anticosti Basin, as well as in Ordovician/Silurian boundary sections around the world, physical stratigraphic evidence suggests that the main phase of sea level fall associated with the Hirnantian Glacial Maximum did not occur until the middle to late Hirnantian (Desrochers et al., 2010; Kiipli and Kiipli, 2020; Calner et al., 2021; Ghienne et al., 2023; Zimmt et al., 2024).

Revision to the timing and stratigraphic position of the Hirnantian Glacial Maximum in the Anticosti Basin, and elsewhere, raises questions as to the veracity of the two-pulse hypothesis of the Late Ordovician mass extinction (LOME). The traditional interpretation of the extinction event attributes the first, and largest, pulse of extinction to global cooling and glacio-eustatic fall at the Katian/Hirnantian boundary (Sheehan, 2001). Clusters of last occurrences in the fossil record, commonly interpreted as a pulse of extinction, occur at the Katian/Hirnantian boundary in basins around the world: this boundary is often marked by unconformities and/or facies shifts that reflect glacio-eustatic fall at the onset of the intensification of the Early Paleozoic Icehouse (Holland and Patzkowsky, 2015). However, in the expanded Ordovician/Silurian boundary section of the Anticosti Basin, no cluster of last occurrences in the brachiopod fossil record is present at the Katian/Hirnantian boundary and the onset of the first phase of global cooling and glacio-eustatic fall (see Copper et al., 2013; though note the artificial truncation in the ranges of certain species: see data in Jin and Zhan, 2008, and Zimmt et al., 2021). Instead, the first cluster of last occurrences in the Anticosti Basin occurs in the upper, middle Hirnantian part of the Ellis Bay Formation, below the subaerial unconformity that marks the Hirnantian Glacial Maximum when tropical sea surface temperatures cooled and global ice volume increased dramatically.

While clusters of last occurrences may represent genuine pulses of extinction (e.g., indicating a common cause; Peters, 2005), the clustering of last occurrences at major stratigraphic surfaces is predicted irrespective of the underlying pattern of extinction (Holland, 1995, 2020). The last occurrences of taxa in the fossil record can be "backscattered" to older stratigraphic surfaces that predate an extinction event (Holland, 1995; Holland and Patzkowsky, 2015; Nawrot et al., 2018; Zimmt et al., 2021). This effect is seen in Hirnantian sections: for example, intensive sampling at the Vinini Creek Ordovician/Silurian boundary section revealed that graptolite species previously thought to have become extinct at the facies shift marking the Katian/Hirnantian boundary persisted up to the Ordovician/Silurian boundary. These range extensions decreased the number of last occurrences at the Katian/Hirnantian boundary both locally and globally (Mitchell et al., 2007; Štorch et al., 2011). Studies of the global fossil record, however, have found a clear signal of cooling-driven extinction in the Late Ordovician (Vandenbroucke et al., 2010; Finnegan et al., 2012; Saupe et al., 2020). If cooling was indeed a main driver of the LOME, it may have either caused gradual extinctions in marine taxa as the icehouse reached its peak (e.g., Sheets et al., 2016) or as a pulse of extinction associated with the Hirnantian Glacial Maximum itself, with last occurrences backscattered to older stratigraphic surfaces marking the Katian/Hirnantian boundary (see Zimmt et al., 2021 and sources cited therein). This may help to explain the discrepancy in patterns of last occurrences between the Anticosti Basin and other Ordovician/Silurian boundary sections. Further integrative studies of Ordovician/Silurian boundary sections are therefore essential for clarifying the relationship between Earth system changes and the history of life during this critical interval. Such studies will play a key role in deconvolving the stratigraphic influences that shape both the paleobiological and geochemical records.

CONCLUSIONS

1. When combined, stable isotope ($\delta^{13}C$, $\delta^{18}O$), carbonate clumped isotope (Δ_{47}), and trace and minor element data (ICP-OES, μXRF) can be used to identify fossils that primarily experienced low water:rock ratio alteration (e.g., sediment-buffered alteration, solid-state reordering). However, burial history estimates suggest that solid-state reordering may have influenced the final Δ_{47} signature of fossils from the Ellis Bay Formation and cannot be entirely ruled out. Leveraging this integrative approach for identifying well-preserved fossils produces well-constrained isotopic profiles for the Ellis Bay Formation.

2. Rugose corals from the Ellis Bay Formation record two intervals of increasing $\delta^{18}O_{VPDB}$ values. The first is in the Fraise Member, just above the Vaureal/Ellis Bay contact (1.0‰–1.5‰), and the second is across the base of the Laframboise Member (2.5‰–4.5‰). Both intervals can be assigned to the Hirnantian Stage based on an assessment of chemostratigraphic, biostratigraphic, paleobiological, sedimentological, and sequence stratigraphic evidence.

3. Compared to our Katian reference frame, the Hirnantian Glacial Maximum marks a $\delta^{18}O_{VPDB}$ excursion of 4‰–5‰ in the Anticosti Basin. In contrast to previous work, which considered the Laframboise Member a representative record of the Hirnantian Glacial Maximum, stratigraphic, $\delta^{18}O$, and Δ_{47} data suggest that the Laframboise Member was deposited in the middle to late Hirnantian following the Hirnantian Glacial Maximum, despite the continued presence of large Gondwanan ice sheets and cool tropical temperatures. This should supplant the interpretation from previous studies (e.g., Finnegan et al., 2012).

4. A middle to late Hirnantian timing of the Hirnantian Glacial Maximum apparently contradicts the two-pulse model of the LOME, which attributes a pulse of extinction to rapid global cooling and glacio-eustatic fall at the Katian/Hirnantian boundary. When combined with insight from the fossil record, patterns of fossil occurrences suggest that the first pulse of extinction may have occurred as late as the Hirnantian Glacial Maximum. These new data thus challenge the notion that the pri-

mary pulse of the LOME occurs at the Katian/Hirnantian boundary.

ACKNOWLEDGMENTS

We thank the David and Lucile Packard Foundation's support to both Bergmann and Finnegan for field and laboratory expenses; the Fonds de recherche du Québec (FRQ-Anticosti program) support to Zimmt; Roger Creel, Matt Braun, Jon Husson, and Mariko Cappello for their expertise and assistance with fieldwork; Diane Erwin for her assistance with the preparation and mounting of fossils; Fran Meyer for her work on the clumped isotope analyses at the Massachusetts Institute of Technology; Bryce Barney for his help in comparing our results to those of previous studies; and the community of Port-Menier for their support and assistance throughout this project.

REFERENCES CITED

Achab, A., Asselin, E., Desrochers, A., Riva, J.F., and Farley, C., 2011, Chitinozoan contribution to the development of a new Upper Ordovician stratigraphic framework for Anticosti Island: Geological Society of America Bulletin, v. 123, p. 186–205, https://doi.org/10.1130/B30131.1.

Achab, A., Asselin, E., Desrochers, A., and Riva, J.F., 2013, The end-Ordovician chitinozoan zones of Anticosti Island, Québec: Definition and stratigraphic position: Review of Palaeobotany and Palynology, v. 198, p. 92–109, https://doi.org/10.1016/j.revpalbo.2012.07.019.

Ahm, A.-S.C., Bjerrum, C.J., and Hammarlund, E.U., 2017, Disentangling the record of diagenesis, local redox conditions, and global seawater chemistry during the latest Ordovician glaciation: Earth and Planetary Science Letters, v. 459, p. 145–156, https://doi.org/10.1016/j.epsl.2016.09.049.

Ahm, A.-S.C., Bjerrum, C.J., Blätter, C.L., Swart, P.K., and Higgins, J.A., 2018, Quantifying early marine diagenesis in shallow-water carbonate sediments: Geochimica et Cosmochimica Acta, v. 236, p. 140–159, https://doi.org/10.1016/j.gca.2018.02.042.

Ainsaar, L., Kaljo, D., Martma, T., Meidla, T., Männik, P., Nõlvak, J., and Tinn, O., 2010, Middle and Upper Ordovician carbon isotope chemostratigraphy in Baltoscandia: A correlation standard and clues to environmental history: Palaeogeography, Palaeoclimatology, Palaeoecology, v. 294, p. 189–201, https://doi.org/10.1016/j.palaeo.2010.01.003.

Anderson, N.T., et al., 2021, A unified clumped isotope thermometer calibration (0.5–1,100°C) using carbonate-based standardization: Geophysical Research Letters, v. 48, https://doi.org/10.1029/2020GL092069.

Armstrong, H.A., and Coe, A.L., 1997, Deep-sea sediments record the geophysiology of the Late Ordovician Glaciation: Journal of the Geological Society, v. 154, p. 929–934, https://doi.org/10.1144/gsjgs.154.6.0929.

Banner, J.L., and Hanson, G.N., 1990, Calculation of simultaneous isotopic and trace element variations during water-rock interaction with applications to carbonate diagenesis: Geochimica et Cosmochimica Acta, v. 54, p. 3123–3137, https://doi.org/10.1016/0016-7037(90)90128-8.

Barnes, C.R., 1988, Stratigraphy and palaeontology of the Ordovician–Silurian boundary interval, Anticosti Island, Quebec, Canada: Bulletin of the British Museum, Natural History (Geology), v. 43, p. 195–219, https://biostor.org/reference/118576.

Barney, B.B., and Grossman, E.L., 2022, Reassessment of ocean paleotemperatures during the Late Ordovician: Geology, v. 50, p. 572–576, https://doi.org/10.1130/G49422.1.

Bartlett, R., Elrick, M., Wheeley, J.R., Polyak, V., Desrochers, A., and Asmerom, Y., 2018, Abrupt global-ocean anoxia during the Late Ordovician–early Silurian detected using uranium isotopes of marine carbonates: Proceedings of the National Academy of Sciences of the United States of America, v. 115, p. 5896–5901, https://doi.org/10.1073/pnas.1802438115.

Bergmann, K.D., Al Balushi, S.A.K., Mackey, T.J., Grotzinger, J.P., and Eiler, J.M., 2018, A 600-million year carbonate clumped-isotope record from the Sultanate of Oman: Journal of Sedimentary Research, v. 88, p. 960–979, https://doi.org/10.2110/jsr.2018.51.

Bergmann, K.D., Macdonald, F.A., and Swanson-Hysell, N.L., 2025, The causes and consequences of Ordovician cooling: Annual Review of Earth and Planetary Sciences, v. 53, https://doi.org/10.1146/annurev-earth-040523-114630.

Bergström, S.M., Young, S., and Schmitz, B., 2010, Katian (Upper Ordovician) $\delta^{13}C$ chemostratigraphy and sequence stratigraphy in the United States and Baltoscandia: A regional comparison: Palaeogeography, Palaeoclimatology, Palaeoecology, v. 296, p. 217–234, https://doi.org/10.1016/j.palaeo.2010.02.035.

Bergström, S.M., Kleffner, M., Schmitz, B., and Cramer, B.D., 2011, Revision of the position of the Ordovician–Silurian boundary in southern Ontario: Regional chronostratigraphic implications of $\delta^{13}C$ chemostratigraphy of the Manitoulin Formation and associated strata: Canadian Journal of Earth Sciences, v. 48, p. 1447–1470, https://doi.org/10.1139/e11-039.

Bergström, S.M., Saltzman, M.R., Leslie, S.A., Ferretti, A., and Young, S.A., 2015, Trans-Atlantic application of the Baltic Middle and Upper Ordovician carbon isotope zonation: Estonian Journal of Earth Sciences, v. 64, p. 8–12, https://doi.org/10.3176/earth.2015.02.

Bergström, S.M., Kleffner, M., and Eriksson, M.S., 2020, Upper Katian (Upper Ordovician) trans-Atlantic $\delta^{13}C$ chemostratigraphy: The geochronological equivalence of the ELKHORN and PAROVEJA excursions and its implications: Lethaia, v. 53, p. 199–216, https://doi.org/10.1111/let.12351.

Bernasconi, S.M., Müller, I.A., Bergmann, K.D., Breitenbach, S.F.M., Fernandez, A., Hodell, D.A., Jaggi, M., Meckler, A.N., Millan, I., and Ziegler, M., 2018, Reducing uncertainties in carbonate clumped isotope analysis through consistent carbonate-based standardization: Geochemistry, Geophysics, Geosystems, v. 19, p. 2895-2914, https://doi.org/10.1029/2017gc007385.

Bernasconi, S.M., et al., 2021, InterCarb: A community effort to improve interlaboratory standardization of the carbonate clumped isotope thermometer using carbonate standards: Geochemistry, Geophysics, Geosystems, v. 22, https://doi.org/10.1029/2020GC009588.

Bertrand, R., 1990, Maturation thermique et histoire de l'enfouissement et de la génération des hydrocarbures du bassin de l'archipel de Mingan et de l'île d'Anticosti, Canada: Canadian Journal of Earth Sciences, v. 27, p. 731–741, https://doi.org/10.1139/e90-075.

Blanchon, P., and Chutcharavan, P., 2023, Meltwater Pulse 1a drowned fringing reefs around Tahiti 15,000 years ago: Royal Society Open Science, v. 10, https://doi.org/10.1098/rsos.230918.

Bolton, T.E., 1981, Ordovician and Silurian biostratigraphy, Anticosti Island, Québec, *in* Lespérance, P.J., ed., International Union of Geological Sciences (IUGS) Field Meeting, Anticosti-Gaspe, Quebec, Vol. 2, Stratigraphy and Paleontology: Montreal, Université de Montréal, IUGS Subcommission on Silurian Stratigraphy, Ordovician-Silurian Boundary Working Group, p. 41–59.

Bond, D.P.G., and Grasby, S.E., 2020, Late Ordovician mass extinction caused by volcanism, warming, and anoxia, not cooling and glaciation: Geology, v. 48, p. 777–781, https://doi.org/10.1130/G47377.1.

Bordet, E., Malo, M., and Kirkwood, D., 2010, A structural study of western Anticosti Island, St. Lawrence platform, Québec: A fracture analysis that integrates surface and subsurface structural data: Bulletin of Canadian Petroleum Geology, v. 58, p. 36–55, https://doi.org/10.2113/gscpgbull.58.1.36.

Brand, U., 1981, Mineralogy and chemistry of the lower Pennsylvanian Kendrick fauna, eastern Kentucky, 1. Trace elements: Chemical Geology, v. 32, p. 1–16, https://doi.org/10.1016/0009-2541(81)90124-8.

Brand, U., 1983, Mineralogy and chemistry of the lower Pennsylvanian Kendrick fauna, eastern Kentucky, U.S.A., 3. Diagenetic and paleoenvironmental analysis: Chemical Geology, v. 40, p. 167–181, https://doi.org/10.1016/0009-2541(83)90097-9.

Brand, U., 2004, Carbon, oxygen, and strontium isotopes in Paleozoic carbonate components: An evaluation of original seawater-chemistry proxies: Chemical Geology, v. 204, p. 23–44, https://doi.org/10.1016/j.chemgeo.2003.10.013.

Brand, U., and Veizer, J., 1980, Chemical diagenesis of a multicomponent carbonate system; 1: Trace elements: Journal of Sedimentary Petrology (now Journal of Sedimentary Research), v. 50, p. 1219–1236, https://doi.org/10.1306/212f7bb7-2b24-11d7-8648000102c1865d.

Brand, U., and Veizer, J., 1981, Chemical diagenesis of a multicomponent carbonate system; 2: Stable isotopes: Journal of Sedimentary Petrology (now Journal of Sedimentary Research), v. 51, p. 987–997, https://doi.org/10.1306/212F7DF6-2B24-11D7-8648000102C1865D.

Brenchley, P.J., and Štorch, P., 1989, Environmental changes in the Hirnantian (upper Ordovician of the Prague basin, Czechoslovakia: Geological Journal, v. 24, p. 165–181, https://doi.org/10.1002/gj.3350240302.

Brenchley, P.J., Marshall, J.D., Carden, G.A.F., Robertson, D.B.R., Long, D.G.F., Meidla, T., Hints, L., and Anderson, T.F., 1994, Bathymetric and isotopic evidence for a short-lived late Ordovician glaciation in a greenhouse period: Geology, v. 22, p. 295–298, https://doi.org/10.1130/0091-7613(1994)022<0295:BAIEFA>2.3.CO;2.

Brenchley, P.J., Carden, G.A., Hints, L., Kaljo, D., Marshall, J.D., Martma, T., Meidla, T., and Nõlvak, J., 2003, High-resolution stable isotope stratigraphy of Upper Ordovician sequences: Constraints on the timing of bioevents and environmental changes associated with mass extinction and glaciation: Geological Society of America Bulletin, v. 115, p. 89–104, https://doi.org/10.1130/0016-7606(2003)115<0089:HRSISO>2.0.CO;2.

Calner, M., Lehnert, O., and Joachimski, M., 2010, Carbonate mud mounds, conglomerates, and sea-level history in the Katian (Upper Ordovician) of central Sweden: Facies, v. 56, p. 157–172, https://doi.org/10.1007/s10347-009-0192-6.

Calner, M., Bockelie, J.F., Rasmussen, C.M.Ø., Calner, H., Lehnert, O., and Joachimski, M.M., 2021, Carbon isotope chemostratigraphy and sea-level history of the Hirnantian Stage (uppermost Ordovician) in the Oslo–Asker district, Norway: Geological Magazine, v. 158, p. 1977–2008, https://doi.org/10.1017/S0016756821000546.

Chen, X., et al., 2006, The Global Boundary Stratotype Section and Point (GSSP) for the base of the Hirnantian Stage (the uppermost of the Ordovician System): Episodes, v. 29, p. 183–196, https://doi.org/10.18814/epiiugs/2006/v29i3/004.

Cocks, L.R.M., and Torsvik, T.H., 2021, Ordovician palaeogeography and climate change: Gondwana Research, v. 100, p. 53–72, https://doi.org/10.1016/j.gr.2020.09.008.

Copper, P., 2001, Reefs during the multiple crises towards the Ordovician–Silurian boundary: Anticosti Island, eastern Canada, and worldwide: Canadian Journal of Earth Sciences, v. 38, p. 153–171, https://doi.org/10.1139/e00-071.

Copper, P., and Jin, J., 2014, The revised Lower Silurian (Rhuddanian) Becscie Formation, Anticosti Island, eastern Canada records the tropical marine faunal recovery from the end-Ordovician Mass Extinction: Newsletters on Stratigraphy, v. 47, p. 61–83, https://doi.org/10.1127/0078-0421/2014/0040.

Copper, P., and Jin, J., 2017, Early athyride brachiopod evolution through the Ordovician–Silurian mass extinction and recovery, Anticosti Island, eastern Canada: Journal of Paleontology, v. 91, p. 1123–1147, https://doi.org/10.1017/jpa.2017.74.

Copper, P., Jin, J., and Desrochers, A., 2013, The Ordovician–Silurian boundary (late Katian–Hirnantian) of western Anticosti Island: Revised stratigraphy and benthic megafaunal correlations: Stratigraphy, v. 10, p. 213–227, https://doi.org/10.29041/strat.10.4.02.

Cronin, T.M., 2012, Rapid sea-level rise: Quaternary Science Reviews, v. 56, p. 11–30, https://doi.org/10.1016/j.quascirev.2012.08.021.

Cummins, R.C., Finnegan, S., Fike, D.A., Eilier, J.M., and Fischer, W.W., 2014, Carbonate clumped isotope

constraints on Silurian ocean temperature and seawater $\delta^{18}O$: Geochimica et Cosmochimica Acta, v. 140, p. 241–258, https://doi.org/10.1016/j.gca.2014.05.024.

Daëron, M., 2021, Full propagation of analytical uncertainties in Δ_{47} measurements: Geochemistry, Geophysics, Geosystems, v. 22, https://doi.org/10.1029/2020GC009592.

Daëron, M., and Vermeesch, P., 2024, Omnivariant Generalized Least Squares regression: Theory, geochronological applications, and making the case for reconciled Δ_{47} calibrations: Chemical Geology, v. 647, https://doi.org/10.1016/j.chemgeo.2023.121881.

Dennis, K.J., Affek, H.P., Passey, B.H., Schrag, D.P., and Eiler, J.M., 2011, Defining an absolute reference frame for 'clumped' isotope studies of CO_2: Geochimica et Cosmochimica Acta, v. 75, p. 7117–7131, https://doi.org/10.1016/j.gca.2011.09.025.

Desrochers, A., and Gauthier, É., 2009, Carte géologique de l'île d'Anticosti (1/250,000): Ministère des Ressources naturelles et de la Faune du Québec (DV 2009-03), scale 1:250,000, 1 sheet.

Desrochers, A., Farley, C., Achab, A., Asselin, E., and Riva, J.F., 2010, A far-field record of the end Ordovician glaciation: The Ellis Bay Formation, Anticosti Island, Eastern Canada: Palaeogeography, Palaeoclimatology, Palaeoecology, v. 296, p. 248–263, https://doi.org/10.1016/j.palaeo.2010.02.017.

Di Celma, C., and Cantalamessa, G., 2007, Sedimentology and high-frequency sequence stratigraphy of a forearc extensional basin: The Miocene Caleta Herradura Formation, Mejillones Peninsula, northern Chile: Sedimentary Geology, v. 198, p. 29–52, https://doi.org/10.1016/j.sedgeo.2006.11.003.

Eiler, J.M., 2011, Paleoclimate reconstruction using carbonate clumped isotope thermometry: Quaternary Science Reviews, v. 30, p. 3575–3588, https://doi.org/10.1016/j.quascirev.2011.09.001.

Elrick, M., Reardon, D., Labor, W., Martin, J., Desrochers, A., and Pope, M., 2013, Orbital-scale climate change and glacioeustasy during the early Late Ordovician (pre-Hirnantian) determined from $\delta^{18}O$ values in marine apatite: Geology, v. 41, p. 775–778, https://doi.org/10.1130/G34363.1.

Fairbanks, R.G., 1989, A 17,000-year glacio-eustatic sea level record: Influence of glacial melting rates on the Younger Dryas event and deep-ocean circulation: Nature, v. 342, p. 637–642, https://doi.org/10.1038/342637a0.

Fielding, C.R., Bann, K.L., MacEachern, J.A., Tye, S.C., and Jones, B.G., 2006, Cyclicity in the nearshore marine to coastal, Lower Permian, Pebbley Beach Formation, southern Sydney Basin, Australia: A record of relative sea-level fluctuations at the close of the Late Palaeozoic Gondwanan ice age: Sedimentology, v. 53, p. 435–463, https://doi.org/10.1111/j.1365-3091.2006.00770.x.

Finnegan, S., Bergmann, K., Eiler, J.M., Jones, D.S., Fike, D.A., Eiseman, I., Hughes, N.C., Tripati, A.K., and Fischer, W.W., 2011, The magnitude and duration of Late Ordovician-Early Silurian Glaciation: Science, v. 331, p. 903–906, https://doi.org/10.1126/science.1200803.

Finnegan, S., Heim, N.A., Peters, S.E., and Fischer, W.F., 2012, Climate change and the selective signature of the Late Ordovician mass extinction: Proceedings of the National Academy of Sciences of the United States of America, v. 109, p. 6829–6834, https://doi.org/10.1073/pnas.1117039109.

Finney, S.C., et al., 1999, Late Ordovician mass extinction: A new perspective from stratigraphic sections in central Nevada: Geology, v. 27, p. 215–218, https://doi.org/10.1130/0091-7613(1999)027<0215:LOMEAN>2.3.CO;2.

Geyman, E.C., and Maloof, A.C., 2021, Facies control on carbonate $\delta^{13}C$ on the Great Bahama Bank: Geology, v. 49, p. 1049–1054, https://doi.org/10.1130/G48862.1.

Ghienne, J.-F., 2003, Late Ordovician sedimentary environments, glacial cycles, and post-glacial transgression in the Taoudeni Basin, West Africa: Palaeogeography, Palaeoclimatology, Palaeoecology, v. 189, p. 117–145, https://doi.org/10.1016/S0031-0182(02)00635-1.

Ghienne, J.-F., Desrochers, A., Vandenbroucke, T.R.A., Achab, A., Asselin, E., Dabard, M.-P., and Farley, C., 2014, A Cenozoic-style scenario for the end-Ordovician glaciation: Nature Communications, v. 5, 4485, https://doi.org/10.1038/ncomms5485.

Ghienne, J.-F., et al., 2023, The Ordovician record of North and West Africa: Unravelling sea-level variations, Gondwana tectonics, and the glacial impact, *in* Servais, T., Harper, D.A.T., and Percival, I.G, eds., A Global Synthesis of the Ordovician System: Part 2: Geological Society, London, Special Publication 533, p. 199–252, https://doi.org/10.1144/SP533-2022-213.

Goldberg, S.L., Present, T.M., Finnegan, S., and Bergmann, K.D., 2021, A high-resolution record of early Paleozoic climate: Proceedings of the National Academy of Sciences of the United States of America, v. 118, https://doi.org/10.1073/pnas.2013083118.

Grossman, E.L., and Joachimski, M.M., 2022, Ocean temperatures through the Phanerozoic reassessed: Scientific Reports, v. 12, https://doi.org/10.1038/s41598-022-11493-1.

Grossman, E.L., Yancey, T.E., Jones, T.E., Bruckschen, P., Chuvashov, B., Mazzullo, S.J., and Mii, H.-s., 2008, Glaciation, aridification, and carbon sequestration in the Permo-Carboniferous: The isotopic record from low latitudes: Palaeogeography, Palaeoclimatology, Palaeoecology, v. 268, p. 222–233, https://doi.org/10.1016/j.palaeo.2008.03.053.

Grossman, E.L., Barney, B.B., Sun, Z., Henkes, G.A., Gao, Y., and Joachimski, M.M., 2025, Cold low-latitude Ordovician paleotemperatures may be in hot water: Proceedings of the National Academy of Sciences of the United States of America, v. 122, https://doi.org/10.1073/pnas.2424291122.

Hammarlund, E.U., et al., 2012, A sulfidic driver for the end-Ordovician mass extinction: Earth and Planetary Science Letters, v. 331–332, p. 128–139, https://doi.org/10.1016/j.epsl.2012.02.024.

Harper, D.A.T., Hammarlund, E.U., and Rasmussen, C.M.Ø., 2014, End Ordovician extinctions: A coincidence of causes: Gondwana Research, v. 25, p. 1294–1307, https://doi.org/10.1016/j.gr.2012.12.021.

Harris, M.T., Sheehan, P.M., Ainsaar, L., Hints, L., Männik, P., Nõlvak, J., and Rubel, M., 2004, Upper Ordovician sequences of western Estonia: Palaeogeography, Palaeoclimatology, Palaeoecology, v. 210, p. 135–148, https://doi.org/10.1016/j.palaeo.2004.02.045.

Hemingway, J.D., and Henkes, G.A., 2021, A disordered kinetic model for clumped isotope bond reordering in carbonates: Earth and Planetary Science Letters, v. 566, https://doi.org/10.1016/j.epsl.2021.116962.

Higgins, J.A., et al., 2018, Mineralogy, early marine diagenesis, and the chemistry of shallow-water carbonate sediments: Geochimica et Cosmochimica Acta, v. 220, p. 512–534, https://doi.org/10.1016/j.gca.2017.09.046.

Hints, L., Hints, O., Kaljo, D., Kiipli, T., Männik, P., Nõlvak, J., and Pärnaste, H., 2010, Hirnantian (latest Ordovician) bio- and chemostratigraphy of the Stirnas-18 core, western Latvia: Estonian Journal of Earth Sciences, v. 59, p. 1–24, https://doi.org/10.3176/earth.2010.1.01.

Holland, S.M., 1995, The stratigraphic distribution of fossils: Paleobiology, v. 21, p. 92–109, https://doi.org/10.1017/S0094837300013099.

Holland, S.M., 2020, The stratigraphic expression of mass extinctions and recoveries: Annual Review of Earth and Planetary Sciences, v. 48, p. 75–97, https://doi.org/10.1146/annurev-earth-071719-054827.

Holland, S.M., and Patzkowsky, M.E., 2015, The stratigraphy of mass extinction: Palaeontology, v. 58, p. 903–924, https://doi.org/10.1111/pala.12188.

Hunt, D., and Tucker, M.E., 1992, Standard parasequences and the forced regressive wedge system tract: Deposition during base level fall: Sedimentary Geology, v. 81, p. 1–9, https://doi.org/10.1016/0037-0738(92)90052-S.

Jablonski, D., 1991, Extinctions: A paleontological perspective: Science, v. 253, p. 754–757, https://doi.org/10.1126/science.253.5021.754.

Jin, J., and Zhan, R., 2008, Late Ordovician Orthide and Billingsellide Brachiopods from Anticosti Island, Eastern Canada: Diversity Change Through Mass Extinction: Ottawa, Ontario, Canada, NRC Research Press, 159 p., https://doi.org/10.1139/9780660197890.

Jones, D.S., Fike, D.A., Finnegan, S., Fischer, W.W., Schrag, D.P., and McCay, D., 2011, Terminal Ordovician carbon isotope stratigraphy and glacioeustatic sea-level change across Anticosti Island (Québec, Canada): Geological Society of America Bulletin, v. 123, p. 1645–1664, https://doi.org/10.1130/B30323.1.

Jones, D.S., Martini, A.M., Fike, D.A., and Kaiho, K., 2017, A volcanic trigger for the Late Ordovician mass extinction?: Mercury data from south China and Laurentia: Geology, v. 45, p. 631–634, https://doi.org/10.1130/G38940.1.

Jones, D.S., Brothers, R.W., Ahm, A.-S.C., Slater, N., Higgins, J.A., and Fike, D.A., 2020, Sea level, carbonate mineralogy, and early diagenesis controlled $\delta^{13}C$ records in Upper Ordovician carbonates: Geology, v. 48, p. 194–199, https://doi.org/10.1130/G46861.1.

Judd, E.J., Bhattacharya, T., and Ivany, L.C., 2020, A dynamical framework for interpreting ancient sea surface temperatures: Geophysical Research Letters, v. 47, https://doi.org/10.1029/2020GL089044.

Judd, E.J., Tierney, J.E., Lunt, D.J., Montañez, I.P., Huber, B.T., Wing, S.L., and Valdes, P.J., 2024, A 485-million-year history of Earth's surface temperature: Science, v. 385, https://doi.org/10.1126/science.adk3705.

Kaljo, D., Hints, L., Martma, T., Nõlvak, J., and Oraspõld, A., 2004, Late Ordovician carbon isotope trend in Estonia, its significance in stratigraphy and environmental analysis: Palaeogeography, Palaeoclimatology, Palaeoecology, v. 210, p. 165–185, https://doi.org/10.1016/j.palaeo.2004.02.044.

Kaljo, D., Hints, L., Männik, P., and Nõlvak, J., 2008, The succession of Hirnantian events based on data from Baltica: Brachiopods, chitinozoans, conodonts, and carbon isotopes: Estonian Journal of Earth Sciences, v. 57, p. 197–218, https://doi.org/10.3176/earth.2008.4.01.

Kaljo, D., Männik, P., Martma, T., and Nõlvak, J., 2012, More about the Ordovician–Silurian transition beds at Mirny Creek, Omulev Mountains, NE Russia: Carbon isotopes and conodonts: Estonian Journal of Earth Sciences, v. 61, p. 277–294, https://doi.org/10.3176/earth.2012.4.07.

Kidwell, S.M., 1997, Anatomy of extremely thin marine sequences landward of a passive-margin hinge zone: Neogene Calvert Cliffs succession, Maryland, U.S.A.: Journal of Sedimentary Research, v. 67, p. 322–340, https://doi.org/10.1306/D4268563-2B26-11D7-8648000102C1865D.

Kiipli, E., and Kiipli, T., 2020, Hirnantian sea-level changes in the Baltoscandian Basin, a review: Palaeogeography, Palaeoclimatology, Palaeoecology, v. 540, https://doi.org/10.1016/j.palaeo.2019.109524.

Kozik, N.P., Gill, B.C., Owens, J.D., Lyons, T.W., and Young, S.A., 2022, Geochemical records reveal protracted and differential marine redox change associated with Late Ordovician climate and mass extinctions: AGU Advances, v. 3, https://doi.org/10.1029/2021AV000563.

Kronenberg, A.K., Yund, R.A., and Giletti, B.J., 1984, Carbon and oxygen diffusion in calcite: Effects of Mn content and PH_2O: Physics and Chemistry of Minerals, v. 11, p. 101–112, https://doi.org/10.1007/BF00309248.

Kump, R.L., Arthur, M.A., Patzkowsky, M.E., Gibbs, M.T., Pinkus, D.S., and Sheehan, P.M., 1999, A weathering hypothesis for glaciation at high atmospheric pCO_2 during the Late Ordovician: Palaeogeography, Palaeoclimatology, Palaeoecology, v. 152, p. 173–187, https://doi.org/10.1016/S0031-0182(99)00046-2.

Li, N., Algeo, T.J., Cheng, M., Jin, C., Zhu, G., Fan, J., and Sun, Z., 2021a, Redox changes in the outer Yangtze Sea (South China) through the Hirnantian Glaciation and their implications for the end-Ordovician biocrisis: Earth-Science Reviews, v. 212, https://doi.org/10.1016/j.earscirev.2020.103443.

Li, P., Duan, J., Cheng, Z., and Zou, H., 2021b, Using clumped isotopes to reconstruct the maximum burial temperature: A case study in the Sichuan Basin: Frontiers of Earth Science, v. 9, https://doi.org/10.3389/feart.2021.759372.

Long, D.G.F., 2007, Tempestite frequency curves: A key to Late Ordovician and Early Silurian subsidence, sea-level change and orbital forcing in the Anticosti foreland basin, Quebec, Canada: Canadian Journal of Earth Sciences, v. 44, p. 413–431, https://doi.org/10.1139/e06-099.

Long, D.G.F., and Copper, P., 1987, Stratigraphy of the Upper Ordovician upper Vaureal and Ellis Bay formations,

eastern Anticosti Island, Quebec: Canadian Journal of Earth Sciences, v. 24, p. 1807–1820, https://doi.org/10.1139/e87-172.

Longman, J., Willis, B.J.W., Manners, H.R., Gernon, T.M., and Palmer, M.R., 2021, Late Ordovician climate change and extinctions driven by elevated volcanic nutrient supply: Nature Geoscience, v. 14, p. 924–929, https://doi.org/10.1038/s41561-021-00855-5.

Looser, N., et al., 2023, Thermally-induced clumped isotope resetting in belemnite and optical calcites: Towards material-specific kinetics: Geochimica et Cosmochimica Acta, v. 350, p. 1–15, https://doi.org/10.1016/j.gca.2023.03.030.

Lu, C., Zou, H., Wang, G., Cong, F., Quan, Y., and Swart, P.K., 2023, Clumped isotopes of paired dolomite and calcite constraining alteration histories of ancient carbonate successions: Chemical Geology, v. 617, https://doi.org/10.1016/j.chemgeo.2022.121264.

Mauviel, A., and Desrochers, A., 2016, A high-resolution, continuous $\delta^{13}C$ record spanning the Ordovician–Silurian boundary on Anticosti Island, eastern Canada: Canadian Journal of Earth Sciences, v. 53, p. 795–801, https://doi.org/10.1139/cjes-2016-0003.

Mauviel, A., Sinnesael, M., and Desrochers, A., 2020, The stratigraphic and geochemical imprints of Late Ordovician glaciation on far-field neritic carbonates, Anticosti Island, eastern Canada: Palaeogeography, Palaeoclimatology, Palaeoecology, v. 543, https://doi.org/10.1016/j.palaeo.2019.109579.

McCracken, A.D., and Barnes, C.R., 1981, Conodont biostratigraphy and paleoecology of the Ellis Bay Formation, Anticosti Island, Quebec, with special reference to Late Ordovician–Early Silurian chronostratigraphy and the systemic boundary, *in* Nowlan, G.S., et al., eds., Late Ordovician Conodonts from the Vauréal Formation, Anticosti Island, Quebec; Conodont Biostratigraphy and Paleoecology of the Ellis Bay Formation, Anticosti Island, Quebec, with Special Reference to Late Ordovician–Early Silurian Chronostratigraphy and the Systematic Boundary: Geological Survey of Canada Bulletin, v. 329, p. 51–134, https://doi.org/10.4095/119430.

McLaughlin, P.I., and Brett, C.E., 2007, Signatures of sea-level rise on the carbonate margin of a Late Ordovician foreland basin: A case study from the Cincinnati Arch, USA: Palaios, v. 22, p. 245–267, https://doi.org/10.2110/palo.2006.p06-106.

McLaughlin, P.I., et al., 2016, Refining 2 km of Ordovician chronostratigraphy beneath Anticosti Island utilizing integrated chemostratigraphy: Canadian Journal of Earth Sciences, v. 53, p. 865–874, https://doi.org/10.1139/cjes-2015-0242.

Melchin, M.J., 2008, Restudy of some Ordovician–Silurian boundary graptolites from Anticosti Island, Canada, and their biostratigraphic significance: Lethaia, v. 41, p. 55–62, https://doi.org/10.1111/j.1502-3931.2007.00045.x.

Melchin, M.J., and Holmden, C., 2006, Carbon isotope chemostratigraphy in Arctic Canada: Sea-level forcing of carbonate platform weathering and implications for Hirnantian global correlation: Palaeogeography, Palaeoclimatology, Palaeoecology, v. 234, p. 186–200, https://doi.org/10.1016/j.palaeo.2005.10.009.

Melchin, M.J., Mitchell, C.E., Holmden, C., and Štorch, P., 2013, Environmental changes in the Late Ordovician–early Silurian: Review and new insights from black shales and nitrogen isotopes: Geological Society of America Bulletin, v. 125, p. 1635–1670, https://doi.org/10.1130/B30812.1.

Mitchell, C.E., Sheets, H.D., Belscher, K., Finney, S.C., Holmden, C., LaPorte, D.F., Melchin, M.J., and Patterson, W.P., 2007, Species abundance changes during mass extinction and the inverse Signor-Lipps effect: Apparently abrupt graptolite mass extinction as an artifact of sampling: Acta Palaeontologica Sinica, v. 46, p. 340–346.

Montañez, I.P., and Poulsen, C.J., 2013, The Late Paleozoic Ice Age: An evolving paradigm: Annual Review of Earth and Planetary Sciences, v. 41, p. 629–656, https://doi.org/10.1146/annurev.earth.031208.100118.

Nawrot, R., Scarponi, D., Azzarone, M., Dexter, T.A., Kusnerik, K.M., Wittmer, J.M., Amorosi, A., and Kowalewski, M., 2018, Stratigraphic signatures of mass extinctions: Ecological and sedimentary determinants: Proceedings of the Royal Society B, Biological Sciences, v. 285, https://doi.org/10.1098/rspb.2018.1191.

Nowlan, G.S., and Barnes, C., 1987, Thermal maturation of Paleozoic strata in Eastern Canada from conodont colour alteration index (CAI) data with implications for burial history, tectonic evolution, hotspot tracks and mineral and hydrocarbon exploration: Geological Survey of Canada Bulletin, v. 367, https://doi.org/10.4095/122453.

Page, A.A., Zalasiewicz, J.A., Williams, M., and Popov, L.E., 2007, Were transgressive black shales a negative feedback modulating glacioeustasy in the Early Paleozoic Icehouse, *in* Haywood, W.M., Gregory, A.M., and Schmidt, D.N., eds., Deep-Time Perspectives on Climate Change: Marrying the Signal from Computer Models and Biological Proxies: London, The Geological Society, The Micropaleontological Society Special Publications, p. 123–156, https://doi.org/10.1144/TMS002.6.

Perez-Beltran, S., Zaheer, W., Sun, Z., Defliese, W.F., Banerjee, S., and Grossman, E.L., 2023, Density functional theory and ab initio molecular dynamics reveal atomistic mechanisms for carbonate clumped isotope reordering: Science Advances, v. 9, https://doi.org/10.1126/sciadv.adf1701.

Peters, S.E., 2005, Geologic constraints on the macroevolutionary history of marine animals: Proceedings of the National Academy of Sciences of the United States of America, v. 102, p. 12,326–12,331, https://doi.org/10.1073/pnas.0502616102.

Peters, S.E., Husson, J.M., and Czaplewski, J., 2018, Macrostrat: A platform for geological data integration and deep-time earth crust research: Geochemistry, Geophysics, Geosystems, v. 19, p. 1393–1409, https://doi.org/10.1029/2018GC007467.

Petryk, A.A., 1981, Stratigraphy, sedimentology, and paleogeography of the Upper Ordovician–Lower Silurian of Anticosti Island Québec, *in* Lespérance, P.J., ed., International Union of Geological Sciences (IUGS) Field Meeting, Anticosti-Gaspe, Quebec, Vol. 2, Stratigraphy and Paleontology: Montreal, Université de Montréal, IUGS Subcommission on Silurian Stratigraphy, Ordovician-Silurian Boundary Working Group, p. 11–39.

Pinet, N., Keating, P., Lavoie, D., Dietrich, J., Duchesne, M.J., and Brake, V., 2012, Revisiting the Appalachian structural front and offshore Anticosti Basin (northern Gulf of St. Lawrence, Canada) by integrating old and new geophysical datasets: Marine and Petroleum Geology, v. 32, p. 50–62, https://doi.org/10.1016/j.marpetgeo.2011.12.004.

Pohl, A., Donnadieu, Y., Le Hir, G., Ladant, J.-B., Dumas, C., Alvarez-Solas, J., and Vandenbroucke, T.R.A., 2016, Glacial onset predated Late Ordovician climate cooling: Paleoceanography, v. 31, p. 800–821, https://doi.org/10.1002/2016PA002928.

Pohl, A., et al., 2021, Vertical decoupling in Late Ordovician anoxia due to reorganization of ocean circulation: Nature Geoscience, v. 14, p. 868–873, https://doi.org/10.1038/s41561-021-00843-9.

Pope, M., and Read, J.F., 1998, Ordovician metre-scale cycles: Implications for climate and eustatic fluctuations in the central Appalachians during a global greenhouse, non-glacial to glacial transition: Palaeogeography, Palaeoclimatology, Palaeoecology, v. 138, p. 27–42, https://doi.org/10.1016/S0031-0182(97)00130-2.

Porębski, S.J., Anczkiewicz, R., Paszkowski, M., Skompski, S., Kędzior, A., Mazur, S., Szczepański, J., Buniak, A., and Mikołajewski, Z., 2019, Hirnantian icebergs in the subtropical shelf of Baltica: Evidence from sedimentology and detrital zircon provenance: Geology, v. 47, p. 284–288, https://doi.org/10.1130/G45777.1.

Porter, S.M., 2010, Calcite and aragonite seas and the *de novo* acquisition of carbonate skeletons: Geobiology, v. 8, p. 256–277, https://doi.org/10.1111/j.1472-4669.2010.00246.x.

Powell, J.W., Schneider, D.A., Desrochers, A., Flowers, R.M., Metcalf, J.R., Gaidies, F., and Stockli, D.F., 2018, Low-temperature thermochronology of Anticosti Island: A case study on the application of conodont (U-Th)/He thermochronology to carbonate basin analysis: Marine and Petroleum Geology, v. 96, p. 441–456, https://doi.org/10.1016/j.marpetgeo.2018.05.018.

Rasmussen, C.M.Ø., Kröger, B., Nielsen, M.L., and Colmenar, J., 2019, Cascading trend of Early Paleozoic marine radiations paused by Late Ordovician extinctions: Proceedings of the National Academy of Sciences of the United States of America, v. 116, p. 7207–7213, https://doi.org/10.1073/pnas.1821123116.

Rasmussen, C.M.Ø., Vandenbroucke, T.R.A., Nogues-Bravo, D., and Finnegan, S., 2023, Was the Late Ordovician mass extinction truly exceptional?: Trends in Ecology & Evolution, v. 38, p. 812–821, https://doi.org/10.1016/j.tree.2023.04.009.

Read, J.F., 1998, Phanerozoic carbonate ramps from greenhouse, transitional, and ice-house worlds: Clues from field and modelling studies, *in* Wright, V.P., and Burchette, T.P., eds., Carbonate Ramps: Geological Society, London, Special Publication 149, p. 107–135, https://doi.org/10.1144/GSL.SP.1999.149.01.07.

Riva, J., 1988, Graptolites at and below the Ordovician–Silurian boundary on Anticosti Island, Canada: Bulletin of the British Museum of Natural History (Geology), v. 43, p. 221–237, https://biostor.org/reference/118577.

Rohrssen, M., Love, G.D., Fischer, W., Finnegan, S., and Fike, D.A., 2013, Lipid biomarkers record fundamental changes in the microbial community structure of tropical seas during the Late Ordovician Hirnantian glaciation: Geology, v. 41, p. 127–130, https://doi.org/10.1130/G33671.1.

Rong, J., and Harper, D.A.T., 1988, A global synthesis of the latest Ordovician Hirnantian brachiopod faunas: Earth and Environmental Science Transactions of the Royal Society of Edinburgh, v. 79, p. 384–402, https://doi.org/10.1017/S026359330001436X.

Rong, J., Xu, C., and Harper, D.A.T., 2002, The latest Ordovician *Hirnantia* fauna (Brachiopoda) in time and space: Lethaia, v. 35, p. 231–249, https://doi.org/10.1111/j.1502-3931.2002.tb00081.x.

Rong, J., Harper, D.A.T., Huang, B., Li, R., Zhang, X., and Chen, D., 2020, The latest Ordovician Hirnantian brachiopod faunas: New global insights: Earth-Science Reviews, v. 208, https://doi.org/10.1016/j.earscirev.2020.103280.

Sami, T., and Desrochers, A., 1992, Episodic sedimentation on an early Silurian, storm-dominated carbonate ramp, Becscie and Merrimack formations, Anticosti Island, Canada: Sedimentology, v. 39, p. 355–381, https://doi.org/10.1111/j.1365-3091.1992.tb02122.x.

Sanford, B.V., 1993, St. Lawrence Platform—Geology, *in* Scott, D.F., and Aitken, J.D., eds., Sedimentary Cover of the Craton in Canada: Geological Survey of Canada, Geology of Canada, v. 5, p. 723–786, https://doi.org/10.1130/DNAG-GNA-D1.723 [also published as Geological Society of America, Geology of North America, v. D-1].

Saupe, E.E., et al., 2020, Extinction intensity during Ordovician and Cenozoic glaciations explained by cooling and palaeogeography: Nature Geoscience, v. 13, p. 65–70, https://doi.org/10.1038/s41561-019-0504-6.

Schuchert, C., and Twenhofel, W.H., 1910, Ordovician–Silurian section of the Mingan and Anticosti islands, Gulf of Saint Lawrence: Geological Society of America Bulletin, v. 21, p. 667–716, https://doi.org/10.1130/GSAB-21-667.

Sheehan, P.M., 2001, The Late Ordovician mass extinction: Annual Review of Earth and Planetary Sciences, v. 29, p. 331–364, https://doi.org/10.1146/annurev.earth.29.1.331.

Sheets, H.D., Mitchell, C.E., Melchin, M.J., Loxton, J., Štorch, P., Carlucci, K.L., and Hawkins, A.D., 2016, Graptolite community responses to global climate change and the Late Ordovician mass extinction: Proceedings of the National Academy of Sciences of the United States of America, v. 113, p. 8380–8385, https://doi.org/10.1073/pnas.1602102113.

Shields, G.A., Carden, G.A.F., Veizer, J., Meidla, T., Rong, J.-Y., and Li, R.Y., 2003, Sr, C, and O isotope geochemistry of Ordovician brachiopods: A major isotopic event around the Middle-Late Ordovician transition: Geochimica et Cosmochimica Acta, v. 67, p. 2005–2025, https://doi.org/10.1016/S0016-7037(02)01116-X.

Sinnesael, M., McLaughlin, P.I., Desrochers, A., Mauviel, A., De Weirdt, J., Claeys, P., and Vandenbroucke, T.R.A., 2021, Precession-driven climate cycles and

time scale prior to the Hirnantian glacial maximum: Geology, v. 49, p. 1295–1300, https://doi.org/10.1130/G49083.1.

Sorauf, J.E., 1997, Geochemical signature of incremental growth and diagenesis of skeletal structure in *Tabulophyllum traversensis* (Winchell, 1866): Bolotin de la Real Sociedad Española de Historia Natural, v. 92, p. 77–86.

Staudigel, P., et al., 2023, Fingerprinting kinetic isotope effects and diagenetic exchange reactions using fluid inclusion and dual-clumped isotope analysis: Geochemistry, Geophysics, Geosystems, v. 24, https://doi.org/10.1029/2022GC010766.

Štorch, P., Mitchell, M.E., Finney, S.C., and Melchin, C.J., 2011, Uppermost Ordovician (upper Katian-Hirnantian) graptolites of north-central Nevada, U.S.A.: Bulletin of Geosciences, v. 86, p. 301–386, https://doi.org/10.3140/bull.geosci.1264.

Swanson-Hysell, N.K., and Macdonald, F.A., 2017, Tropical weathering of the Taconic orogeny as a driver for Ordovician cooling: Geology, v. 45, p. 719–722, https://doi.org/10.1130/G38985.1.

Swart, P.K., 2008, Global synchronous changes in the carbon isotopic composition of carbonate sediments unrelated to changes in the global carbon cycle: Earth, Atmospheric, and Planetary Sciences, v. 105, p. 13,741–13,745, https://doi.org/10.1073/pnas.0802841105.

Temple, J.T., 1965, Upper Ordovician brachiopods from Poland and Britain: Acta Palaeontologica Polonica, v. 10, p. 379–450.

Thiagarajan, N., Lepland, A., Ryb, U., Torsvik, T.H., Ainsaar, L., Hints, O., and Eiler, J., 2024, Reconstruction of Phanerozoic climate using carbonate clumped isotopes and implications for the oxygen isotopic composition of seawater: Proceedings of the National Academy of Sciences of the United States of America, v. 121, https://doi.org/10.1073/pnas.2400434121.

Torsvik, T.H., and Cocks, L.R.M., 2016, Ordovician, *in* Torsvik, T.H., and Cocks, L.R.M., eds., Earth History and Palaeogeography: Cambridge, UK, Cambridge University Press, p. 101–123, https://doi.org/10.1017/9781316225523.007.

Trotter, J.A., Williams, I.S., Barnes, C.R., Lécuyer, C., and Nicoll, R.S., 2008, Did cooling oceans trigger Ordovician biodiversification?: Evidence from conodont thermometry: Science, v. 321, p. 550–554, https://doi.org/10.1126/science.1155814.

Turner, B.R., Armstrong, H.A., Wilson, C.R., and Makhlouf, I.M., 2012, High frequency eustatic sea-level changes during the Middle to early Late Ordovician of southern Jordan: Indirect evidence for a Darriwilian Ice Age in Gondwana: Sedimentary Geology, v. 251–252, p. 34–48, https://doi.org/10.1016/j.sedgeo.2012.01.002.

Ullmann, C.V., and Korte, C., 2015, Diagenetic alteration in low-Mg calcite from macrofossils: A review: Geological Quarterly, v. 59, p. 3–20, https://doi.org/10.7306/gq.1217.

Underwood, C.J., Crowley, S.F., Marshall, J.D., and Brenchley, P.J., 1997, High resolution carbon isotope stratigraphy of the basal Silurian stratotype (Dob's Linn, Scotland) and its global correlation: Journal of the Geological Society, v. 154, p. 709–718, https://doi.org/10.1144/gsjgs.154.4.0709.

Vandenbroucke, T.R.A., Armstrong, H.A., Williams, M., Paris, F., Sabbe, K., Zalasiewicz, J., Nõlvak, J., and Verniers, J., 2010, Epipelagic chitinozoan biotopes map a steep latitudinal temperature gradient for earliest Late Ordovician seas: Implications for a cooling Late Ordovician climate: Palaeogeography, Palaeoclimatology, Palaeoecology, v. 294, p. 202–219, https://doi.org/10.1016/j.palaeo.2009.11.026.

Webb, G.E., and Sorauf, J.E., 2002, Zigzag microstructure in rugose corals: A possible indicator of relative seawater Mg/Ca ratios: Geology, v. 30, p. 415–418, https://doi.org/10.1130/0091-7613(2002)030<0415:ZMIRCA>2.0.CO;2.

Westerhold, T., et al., 2020, An astronomically dated record of Earth's climate and its predictability over the last 66 million years: Science, v. 369, p. 1383–1387, https://doi.org/10.1126/science.aba6853.

Young, S.A., Benayoun, E., Kozik, N.P., Hints, O., Martma, T., Bergström, S.M., and Owens, J.D., 2020, Marine redox variability from Baltica during extinction events in the latest Ordovician–early Silurian: Palaeogeography, Palaeoclimatology, Palaeoecology, v. 554, https://doi.org/10.1016/j.palaeo.2020.109792.

Zachos, J., Pagani, M., Sloan, L., Thomas, E., and Billups, K., 2001, Trends, rhythms, and aberrations in global climate 65 Ma to present: Science, v. 292, p. 686–693, https://doi.org/10.1126/science.1059412.

Zecchin, M., and Catuneanu, O., 2013, High-resolution sequence stratigraphy of clastic shelves I: Units and bounding surfaces: Marine and Petroleum Geology, v. 39, p. 1–25, https://doi.org/10.1016/j.marpetgeo.2012.08.015.

Zimmt, J.B., and Jin, J., 2023, A new species of Hirnantia (Orthida, Brachiopoda) and its implications for the Hirnantian age of the Ellis Bay Formation, Anticosti Island, eastern Canada: Journal of Paleontology, v. 97, p. 47–62, https://doi.org/10.1017/jpa.2022.83.

Zimmt, J.B., Holland, S.M., Finnegan, S., and Marshall, C.R., 2021, Recognizing pulses of extinction from clusters of last occurrences: Palaeontology, v. 64, p. 1–20, https://doi.org/10.1111/pala.12505.

Zimmt, J.B., Holland, S.M., Desrochers, A., Jones, D.S., and Finnegan, S., 2024, A high-resolution sequence stratigraphic framework for the eastern Ellis Bay Formation, Canada: A record of Hirnantian sea-level change: Geological Society of America Bulletin, v. 136, p. 3825–3849, https://doi.org/10.1130/B37190.1.

Zou, C., et al., 2018, Ocean euxinia and climate change "double whammy" drove the Late Ordovician mass extinction: Geology, v. 46, p. 535–538, https://doi.org/10.1130/G40121.1.

Science Editor: Troy Rasbury
Associate Editor: Gregory Henkes

Manuscript Received 14 July 2024
Revised Manuscript Received 29 April 2025
Manuscript Accepted 30 May 2025